Journal of Inorganic Biochemistry 199 (2019) 110785

Contents lists available at ScienceDirect

Journal of Inorganic Biochemistry

journal homepage: www.elsevier.com/locate/jinorgbio

Design, synthesis, and anticancer activity of iridium(III) complex-peptide hybrids that contain hydrophobic acyl groups at the *N*-terminus of the peptide units

Kana Naito[a], Kenta Yokoi[a], Chandrasekar Balachandran[a], Yosuke Hisamatsu[a], Shin Aoki[a,b,c,*]

[a] Faculty of Pharmaceutical Sciences, Tokyo University of Science, 2641 Yamazaki, Noda, Chiba 278-8510, Japan
[b] Division of Medical-Science-Engineering Cooperation, Research Institute for Science and Technology, Tokyo University of Science, 2641 Yamazaki, Noda, Chiba 278-8510, Japan
[c] Imaging Frontier Center, Research Institute for Science and Technology, Tokyo University of Science, 2641 Yamazaki, Noda, Chiba 278-8510, Japan

A B S T R A C T

In previous work, we reported on that Ir complex-cationic peptide hybrids (IPHs) that contain three KKGG or KKKGG sequences (K: lysine, G: glycine) induce cell death in cancer cells by an intracellular Ca^{2+}-dependent pathway and function as luminescent detectors in dead cells. To identify the target biomolecules by photoaffinity labeling, we designed and synthesized IPH that contains a photoreactive and hydrophobic 4-[3-(trifluotomethyl)-*3H*-diazirine-3-yl]benzoyl (TFDB) group and found that it has more potent cytotoxicity against Jurkat cells than the previously prepared compounds. Herein, we report on the preparation of some new IPHs that contain hydrophobic acyl groups at the *N*-terminus of the peptide portions of the molecules. Among them, an IPH containing a *n*-dodecanoyl group was found to have much more potent cancer cell death activity and superior selectivity for cancer cells (Jurkat cells) over normal cells. The results of mechanistic studies suggest that the cell death of Jurkat cells is induced via different pathway from that induced by the previously synthesized IPHs. The results of this study are described herein.

1. Introduction

Cyclometalated Ir(III) complexes such as *fac*-Ir(tpy)$_3$ **1a** (tpy: 2-(4′-tolyl)pyridine) and *fac*-Ir(ppy)$_3$ **1b** (ppy: 2-phenylpyridine) have stable and C_3-symmetric structures and excellent photophysical properties, making them useful as phosphorescence materials [1–15]. We previously reported on the design and synthesis of some C_3-symmetric and luminescent Ir complex-peptide hybrids (IPHs) for use as anticancer agents that kill cancer cells via activating different cell death signaling pathways (Scheme 1) [16–20]. The first type of our IPHs were artificial death ligands **2a,b** that mimic a tumor necrosis factor related apoptosis inducing ligand (TRAIL) which contains a cyclic peptide sequence, WDCLDNRIGRRQCVKL (W: tryptophan, D: aspartic acid, C: cysteine, L: leucine, N: asparagine, R: arginine, I: isoleucine, G: glycine, Q: glutamine, V: valine, and K: lysine) that had been reported to bind to death receptor 5 (DR5) [16,17]. In **2b**, a hydrophilic SGSG (S: serine) peptide sequence was introduced between the Ir complex core and the side chain of lysine contained in the cyclic portion to change the linker length with minimal effect on its solubility in water. It was reported that **2a** and **2b** induced the necrosis-like and apoptotic cell death of T-lymphocyte leukemia Jurkat cells, respectively.

The second type includes cationic amphiphilic Ir complexes that contain KKGG or KKKGG sequences with net charge of +9 and +12 through the appropriate alkyl (C6 and C8) linkers and induce the death of Jurkat cells (Scheme 1) [18,19]. Ir complexes **3a** and **3b** containing KKGG peptides at the 5′-position of the tpy moiety (*p*-position with respect to the C—Ir bond) have considerable cytotoxicity against Jurkat cells (a human T-lymphoma cell line), which is accompanied with an apparent morphological change (EC_{50} (half-maximal effective concentration) = 16 μM (**3a**) and 7.3 μM (**3b**)), and they emit a strong green emission in dead cells. At the same time, it was found that **3c**, which contains a C16 linker, has a much weaker cytotoxicity. Therefore, an appropriate cationic charge of the peptide parts and the length of linkers between the Ir complex core and the peptide portion are important factors for their cytotoxicity and suggest that these Ir complexes interact with specific biomolecules on/in the cancer cells. In addition, cell death induced by **3a** is cancelled by some agents that inhibit Ca^{2+}-related intracellular signaling pathways, indicating that cationic amphiphilic Ir complexes induce cell death via a Ca^{2+}-dependent pathway.

In order to isolate and characterize the target molecules of Ir complexes, we attempted photoaffinity labeling by means of **4** equipped

* Corresponding author at: Faculty of Pharmaceutical Sciences, Tokyo University of Science, 2641 Yamazaki, Noda, Chiba 278-8510, Japan.
E-mail address: shinaoki@rs.noda.tus.ac.jp (S. Aoki).
URL: http://www.rs.noda.tus.ac.jp/aokilab/ (S. Aoki).

https://doi.org/10.1016/j.jinorgbio.2019.110785
Received 1 May 2019; Received in revised form 15 July 2019; Accepted 16 July 2019
Available online 03 August 2019
0162-0134/

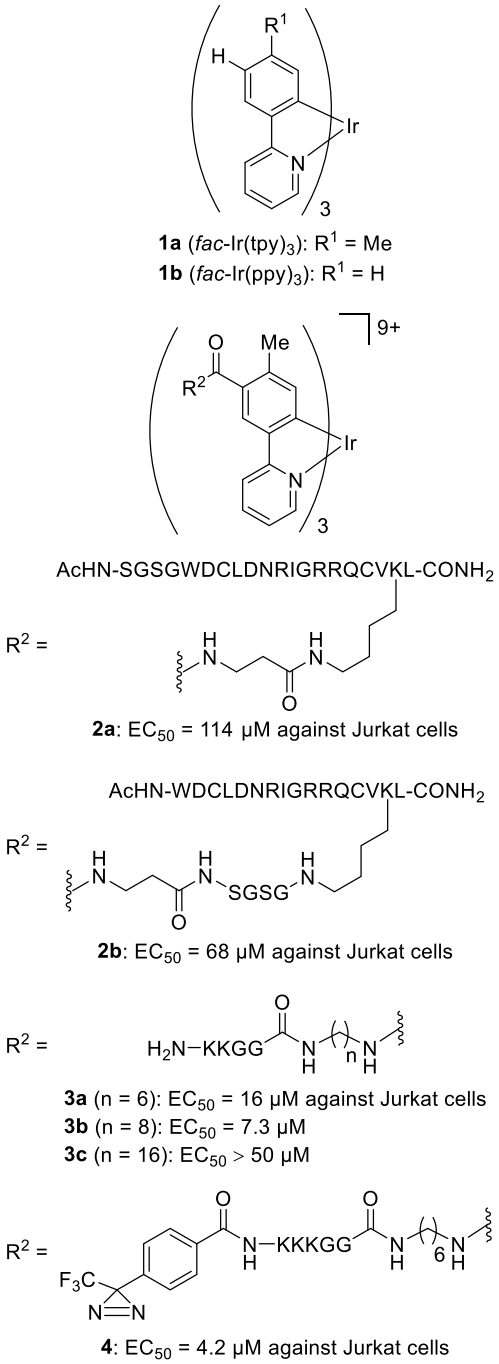

Scheme 1. The structures of cationic amphiphilic Ir complexes derived from Ir(tpy)$_3$ **1a** and their EC_{50} values against Jurkat cells.

with a 4-[3-(trifluoromethyl)-*3H*-diazirine-3-yl]benzoyl (TFDB) unit as a photoreactive group at the *N*-terminus of the KKKGG peptide chain (three lysine residues were inserted in order to adjust the total cationic charge of **4** to +9, similar to that for **3a** and **3b** (+9)). A proteomic analysis of the products after the photoirradiation of Jurkat cells in the presence of **4** suggested that calmodulin (CaM), Ca^{2+}-binding protein, is one of the target proteins.

More interesting information regarding the aforementioned work was that **4** had a more potent cytotoxicity (EC_{50} = 4.2 μM) than **3a**, which contains the same alkyl linker length [19]. This information prompted us to design and synthesize a new series of IPHs that have hydrophobic acyl groups like TFDB unit at the *N*-terminus of the KKKGG peptide units in an attempt to improve their cytotoxicity

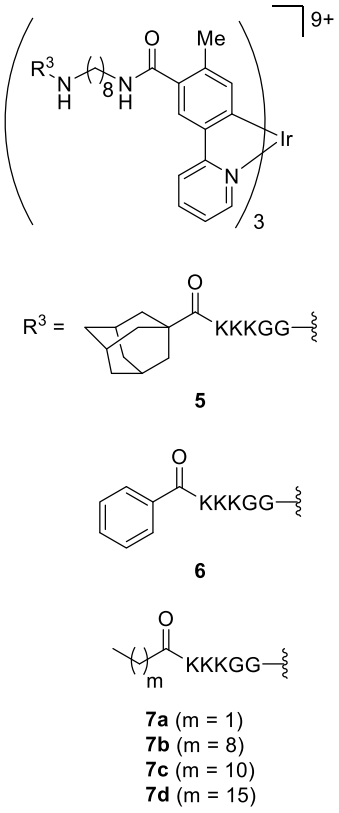

Scheme 2. Ir complexes containing hydrophobic acyl groups at the *N*-terminus of the cationic peptide region.

against cancer cells. In this study, we report on the synthesis of IPHs that contain a 1-adamantyl carbonyl group (**5**), a benzoyl group (**6**), and alkyl chains such as *n*-propionyl (**7a**), *n*-decanoyl (**7b**), *n*-dodecanoyl (**7c**), and *n*-heptadecanoyl (**7d**) and assessments of their cytotoxicity against Jurkat cells (Scheme 2). It has been reported that **5–7d** containing C8 alkyl linkers between the Ir scaffold and the peptide units exhibit a more potent cytotoxicity than **3a** like **4**. It should also be noted that **7a-d** induce cancer cell death via different mechanisms from those of our previous Ir complexes, **2a**,**b** and **3a**,**b** based on a detailed mechanistic study. It also appears that the anticancer effects of **5**, **6**, **7a**, and **7b** are selective against Jurkat cells rather than normal cells. These results are presented and discussed.

2. Result and discussion

2.1. Synthesis of IPHs with N-terminal hydrophobic acyl groups on the cationic regions

The scheme for the synthesis of Ir complexes **5–7** is shown in Scheme 3. The central Ir(tpy)$_3$ unit with C8 linkers (**8**) at the 5′-position of the tpy ligand was synthesized from **1a** (as a racemic mixture (*Δ* and *Λ* form)), as described in a previous paper [18,19,21]. The Boc (tert-butyloxycarbonyl) protected peptides **9a**, **10a**, **11a**, **12a**, **13**, and **14a** were prepared by Fmoc solid-phase peptide synthesis and coupled with **8** to give the corresponding Ir complexes. The last step in the preparation of **14a** was carried out in DMF/CH_2Cl_2 (1:1) due to low solubility of *n*-heptadecanoic acid in DMF alone. Finally, the Boc groups were removed by treatment with trimethylsilyl chloride (TMSCl) and NaI in MeCN [18–22], and the resulting products were purified by reversed-phase high performance liquid chromatography (RP-HPLC) to give the trifluoroacetic acid (TFA) salts of **5–7d** as yellow solids. It should be noted that diastereomers of these Ir complexes resulting from the racemic Ir complex center (*Δ* and *Λ* form) were not detected in ^1H

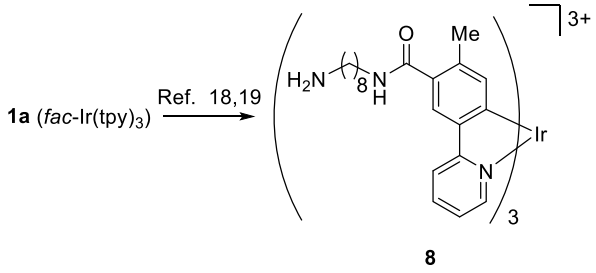

8

1) Protected peptide **9a-14a**,*
PyBOP, DIEA, DMF

2) TMSCl, NaI,CH_3CN

5: 24% from **8** and **9a**
6: 8% from **8** and **10a**
7a: 40% from **8** and **11a**
7b: 29% from **8** and **12a**
7c: 30% from **8** and **13**
7d: 29% from **8** and **14a**

*Peptides

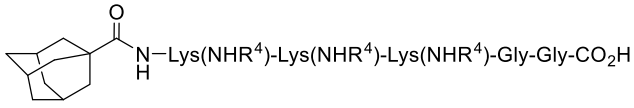

9a: R^4 = Boc
9b: R^4 = H

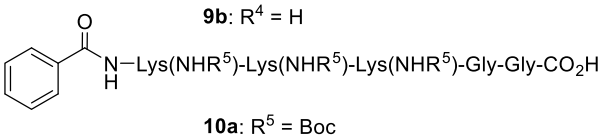

10a: R^5 = Boc
10b: R^5 = H

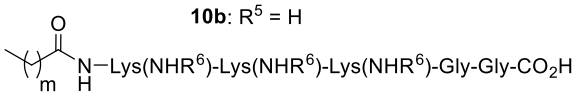

11a (m = 1): R^6 = Boc
11b (m = 1): R^6 = H
12a (m = 8): R^6 = Boc
12b (m = 8): R^6 = H
13 (m = 10): R^6 = Boc
14a (m = 15): R^6 = Boc
14b (m = 15): R^6 = H

Scheme 3. Synthesis of Ir complexes containing cationic peptides.

NMR spectra and hence were not separated. The deprotected peptides **9b**, **10b**, **11b**, **12b**, and **14b** were synthesized by the deprotection of the corresponding protected peptides with a TFA cocktail (TFA/H_2O/triisopropylsilane) and purified by RP-HPLC.

2.2. Photophysical properties of Ir complexes

UV/vis and luminescent spectra of the Ir complexes **5**–**7d** (10 μM) in degassed 100 mM *N*-(2-hydroxyethyl)piperazine-*N*′-2-ethanesulfonic acid (HEPES) at pH 7.4 and 25 °C are shown in Fig. 1 and their photophysical data are summarized in Table 1 along with those of **1a** (in CH_2Cl_2) and **3a**. The concentrations of these Ir complexes in stock solutions (PBS) were determined by our previous method which is based on the molar extinction coefficient at 380 nm ($\varepsilon_{380\ nm}$ = (1.08 ± 0.07) × $10^4\ M^{-1}\ cm^{-1}$) of Ir complex **15** having a C6 diamine linker (Scheme 4) that was characterized by elemental analysis. The UV/vis and emission spectra of **5**, **6**, and **7a**–**d** were nearly identical to that for **3a** (Fig. 1a). The strong absorption bands at ca. 280 nm were assigned

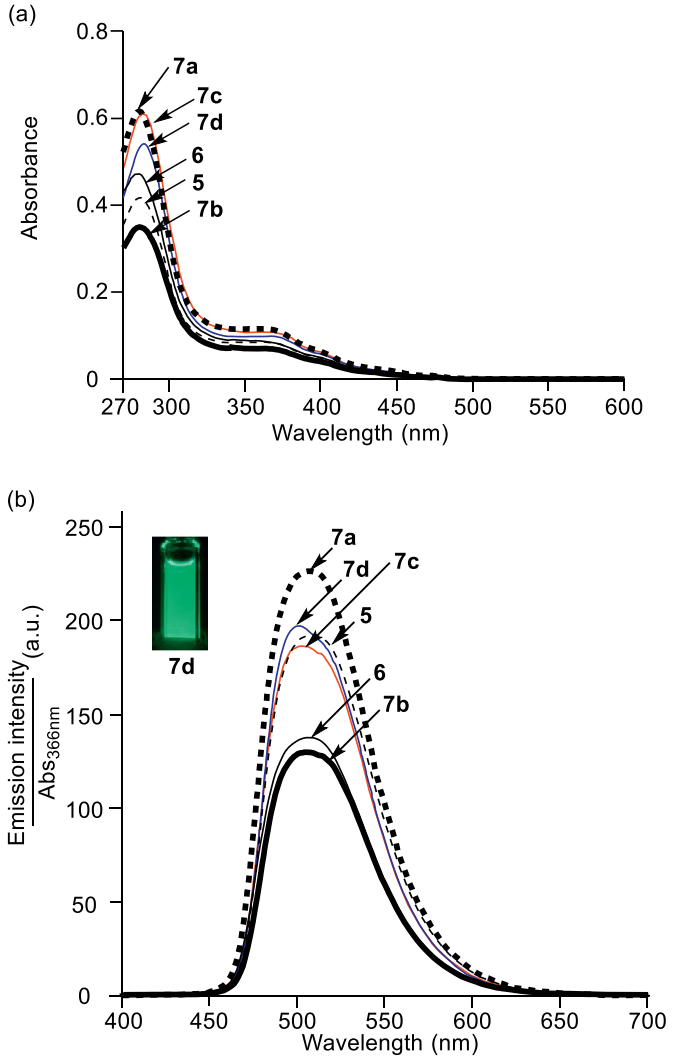

Fig. 1. (a) UV/vis absorption spectra and (b) emission spectra of **5** (black dashed curve), **6** (black plain curve), **7a** (bold black dashed curve), **7b** (bold black curve), **7c** (red plain curve), **7d** (blue plain curve) in degassed 100 mM HEPES (pH = 7.4) at 25 °C. ([Ir complex] = 10 μM, excitation at 366 nm). A.u. is arbitrary units. A photograph shows the emission of **7d** (excitation at 365 nm). (For interpretation of the references to colour in this figure legend, the reader is referred to the web version of this article.)

Table 1
Photophysical properties of Ir complexes **5, 6, 7a–7d** ([Ir complex] = 10 μM) in degassed 100 mM HEPES (pH = 7.4) at 25 °C. [a] Ref 21. [b] Ref 18. [c] Quinine sulfate in 0.1 M H_2SO_4 (Φ = 0.55) were used as a reference. [d] Ref 24.

Compound	λ_{max} (absorption)	λ_{max} (emission)	Φ [c]	τ
1a (in CH_2Cl_2)[a]	287 nm, 373 nm	512 nm	0.50	2.0 μs[a,d]
3a[b]	280 nm, 362 nm	509 nm	0.55	1.7 μs
5	281 nm, 362 nm	508 nm	0.54	1.6 μs
6	279 nm, 359 nm	508 nm	0.44	1.2 μs
7a	281 nm, 360 nm	509 nm	0.55	1.6 μs
7b	281 nm, 360 nm	506 nm	0.51	1.2 μs
7c	282 nm, 361 nm	502 nm	0.56	1.1 μs
7d	284 nm, 366 nm	501 nm	0.52	1.4 μs

to the $^1\pi$–π^* transition of the tpy ligands and the weak shoulder bands at ca. 350–500 nm to spin-allowed singlet-to-singlet (^{1}MLCT) transitions, spin-forbidden singlet-to-triplet (^{3}MLCT) transitions, and $^3\pi$–π^* transitions. In luminescent spectra, **5** and **7a**–**d** produced a green emission with a maxima at ca. 509 nm (Fig. 1b) and the luminescent

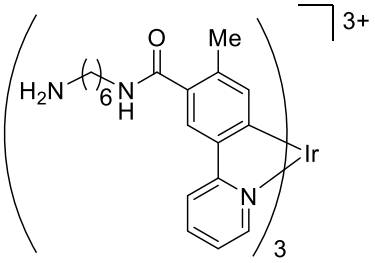

15

Scheme 4. Structure of Ir complex **15** used as a reference to determine the concentration of the Ir complexes in stock solutions (PBS).

quantum yields (Φ) and emission lifetimes (τ) were similar to these for **3a**, as listed in Table 1 [23]. **6** has a smaller emission quantum yield (Φ = 0.44) than those of **3a**, **5**, and **7a–d**. On the other hand, the absorbance peak of **7d** at ca. 280 nm corresponding to the $^1\pi$–π^* transition state was decreased with a small red shift and the emission spectra exhibited a blueshift.

2.3. Cytotoxicity of Ir complexes against Jurkat cells, as evaluated by cell imaging and MTT assays

Morphological changes and bright field and luminescence images of T-lymphocyte leukemia Jurkat cells treated with **5-7d** were observed by luminescence microscopy. The Jurkat cells were incubated in the presence of **5–7d** (50 μM) in Roswell Park Memorial Institute (RPMI)-1640 medium containing 10% fetal bovine serum (FBS) for 1 h at 37 °C under 5% CO_2, then collected by centrifugation (2000 rpm × 3 min), washed with phosphate buffer saline (PBS), and observed by luminescence microscopy (Biorevo, BZ-9000, Keyence). The findings indicated that Ir complexes **5–7** induced the cell death of Jurkat cells with apparent morphological changes and a strong green emission was observed in dead cells, as shown in Fig. 2g–i (for **5**), 2j–l (for **6**), 2 m–o (for **7a**), 2p–r (for **7b**), 2 s–u (for **7c**), and 2v–x (for **7d**), similar to the images of **3a** (Fig. 2d–f) (the emission is localized in the nucleus). When Jurkat cells were treated with **5–7** at 4 °C, these compounds negligibly induced cell death (Fig. 2y–ae), indicating that the cell death induced at 37 °C is dependent on intracellular events that stimulate the cell death pathway. In contrast, the treatment of Jurkat cells with **9b–12b** and **14b**, which are the peptide regions contained in the Ir complexes **5–7b** and **7d**, induced negligible cell death (Fig. 2af–ah) and only **12b** and **14b** (1 mM) induced morphological changes in Jurkat cells, albeit very high concentrations were needed (~1 mM) (Fig. 2 ai and aj). These results suggest that new Ir complexes **5–7d** have a similar or higher cytotoxic activity than **3a**.

The cytotoxicity of the Ir complexes **5–7d** and cationic peptides **9b–12b** and **14b** against Jurkat cells was quantitatively evaluated by means of a 3-(4,5-dimethyl-2-thiazolyl)2,5,-diphenyl-*2H*-tetrazolium bromide (MTT) assay. The viability of Jurkat cells at increasing concentrations of Ir complexes (0–50 μM) and peptides (0–1.0 mM) are shown in Fig. 3, from which the EC_{50} values were determined to be ca. 5–5.4 μM for **5–7a**, 4.4 μM for **7b**, 0.4 μM for **7c**, and 1.0 μM for **7d**, as listed in Table 2, suggesting that the *N*-acylated IPHs **5–7** have more potent cytotoxicity than **3a** and **3b**. The EC_{50} values for the peptide **9b–12b** alone (> 1 mM except for **14b** (40 μM)) are much greater (weaker cytotoxicity) than those of **5–7d**, indicating that the three cationic peptide units with an Ir center core in **5–7d** are important for cell death inducing activity. It should also be pointed out that **7d**, with an C17 acyl group at the *N*-terminus of the peptide regions, had potent anticancer activity against Jurkat cells, while **3c**, which contains a C16 linker between the Ir(tpy)$_3$ core and the peptide portion, had a very weak cytotoxicity.

The effect of **3a–c** and **5–7** on the viability of fibroblastic IMR-90 cells from human fetal lungs, one of the normal cell lines, was also checked by an MTT assay (Fig. 4 and Table 2). The EC_{50} values for **3a–c**, **5**, **6**, **7a**, and **7b** against IMR-90 cells are all in excess of 25 μM, implying that these IPHs are selective to cancer cells. The EC_{50} values of **7c** and **7d** against IMR-90 were 4.2 μM and 7.2 μM, respectively, slightly greater than those against Jurkat cells, suggesting that **7c**,**d** are somewhat selective to cancer cells over normal cells.

2.4. Mechanistic studies of cell death induced by *3a* and *7d*

The strong luminescence of IPHs, which is one of their advantages, allowed us to perform snapshot imaging and follow their behavior in the cell death processes. For more clear imaging of IPHs-treated Jurkat cells, confocal microscopic images were obtained. In Fig. 2d–f, 2p–r, and 2v–x, a strong green emission of **3a**, **7b**, and **7d** (50 μM) was observed on the cell membrane and/or in the cytosol of Jurkat cells after incubation for 1 h. As shown in Figs. 5, **3a**, **7b**, and **d** exhibit different behaviors in cell death processes. The green emission of **3a** moves to the cytosol after a 1 h incubation and then to the membrane and into nucleus after 16 h (Fig. 5a–f). **7b** and **7d** initially accumulate on the cell membrane after 1 h and **7b** then moves into cytosol and nucleus (Fig. 5g–o), while **7d** accumulates on the surface of the nucleus eventually after 16 h (Fig. 5p–x).

We previously determined the intracellular accumulation of **1a** and *N*,*N*-diethylamino-functionalized *fac*-Ir(tpy)$_3$ **16** (Scheme 5), which works as a pH sensor in solutions and a lysosome probe in living HeLa cells, to be 0.27 and 0.20 fmol/cell, respectively, by inductively coupled plasma-mass spectrometer (ICP-MS) [25]. The intracellular uptake of IPHs **7b** and **7d** in Jurkat cells was evaluated by a similar manner. Namely, Jurkat cells were incubated with **7b** or **7d** (10 μM) for 1 or 3 h at 37 °C in 10% FBS containing RPMI medium, washed with PBS, lysed in nitric acid overnight and the resulting samples were analyzed by ICP-MS. The results summarized in Fig. 6 and Table 3 imply that the intracellular uptake of **7b** (0.28 fmol/cell) is almost same as those of **1a** and **16** and it is higher than that of **7d** (0.04 fmol/cell). These data show good agreement with the luminescence images of **7b**- or **7d**-treated Jurkat cells by confocal microscopy displayed in Fig. 5 and the interaction of these Ir complexes with the artificial liposome, which will be discussed below (Fig. 13). Fig. 5j-l and 5s-u show that **7b** is localized on the cell membrane in 1 h and then internalized into the cell after 3 h, resulting in its higher intracellular accumulation, while more hydrophobic **7d** stays on/in the cell membrane even after 3 h. Smaller EC_{50} value (higher cytotoxicity) of **7d** than that of **7b** could be explained by the destabilization and/or decomposition of cell membrane by **7d**, as well as the stimulation of intracellular cell death mechanism by **7d**.

In the following experiments, **3a** and **7d** were mainly used for comparison. Time-lapse imaging (0.5–4 h) of Jurkat cells that were incubated with **3a** (10 μM) and **7d** (1.6 μM) is presented in Fig. 7. These concentrations were determined by MTT assays at different concentrations of **3a** and **7d** (10–50 μM for **3a** and 0–10 μM for **7d**), thus permitting the death of Jurkat cells to be followed by microscopy (data not shown). As shown in Fig. 7a, a green emission of **3a** was observed in the cytosol and cell membrane of Jurkat cells after incubation for 30 min and became largely localized in the cytosol after 1 h. The green emission from **3a** was enhanced considerably after 2–4 h, indicating the death of cells, as supported by the red emission from ethidium bromide (EB) (as shown in the right side pictures of Fig. 7a). It should also be mentioned that the green emission of **3a** in overlay images at 2–4 h is weak, possibly due to fluorescence resonance energy transfer (FRET) from **3a** to EB (because of the overlay of the emission of **3a** and the absorption of EB) (Fig. 7a). In contrast, **7d** was initially localized on the cell membrane and then gradually moved into the cytosol and nearly all of the cells underwent cell death after 2 h (Fig. 7b). Therefore, it can be concluded that **3a** and **7d** induce cell death in 1–2 h, albeit the mechanism responsible for this cell death induced by these two IPHs is somewhat different.

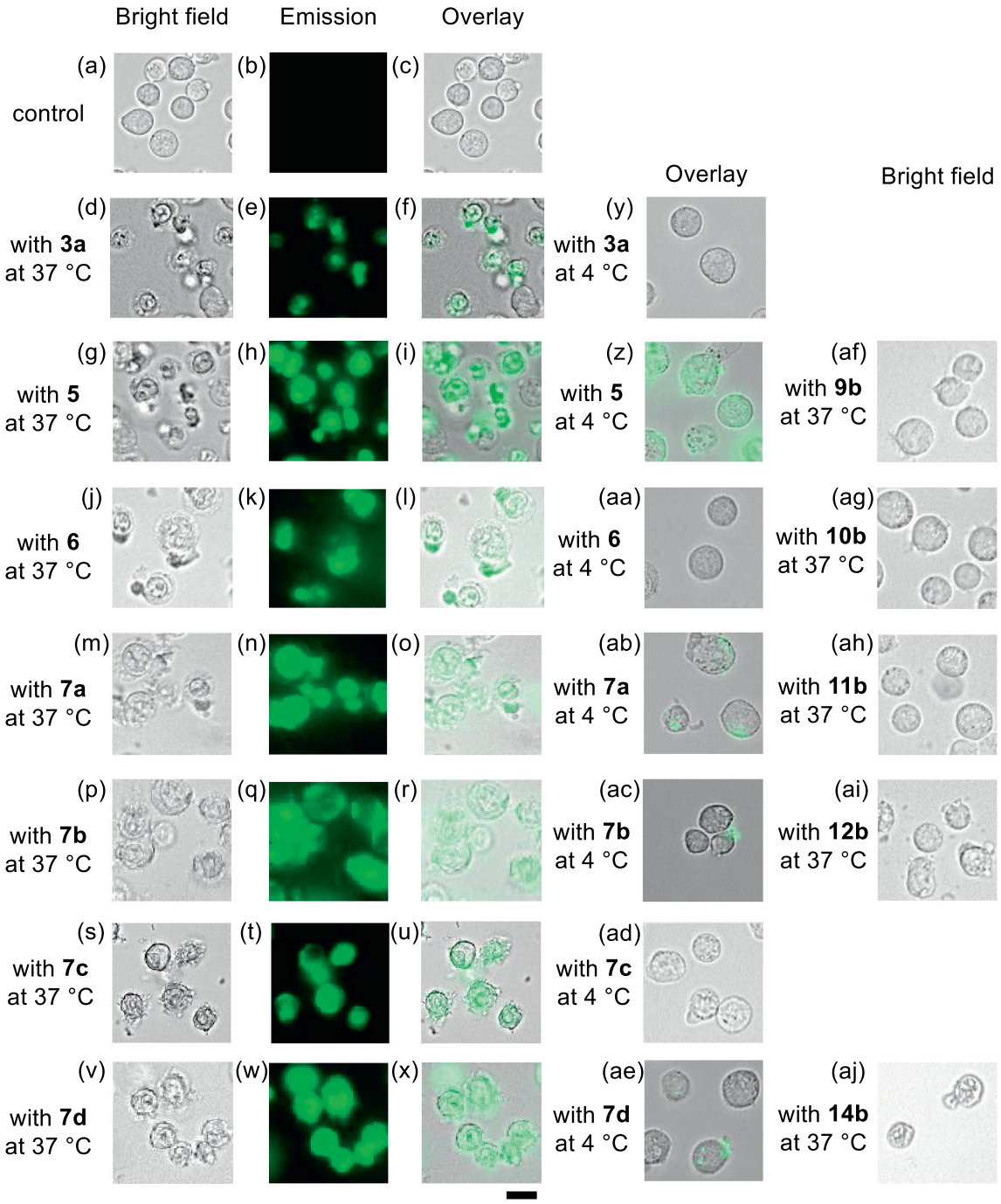

Fig. 2. Typical luminescence microscopic images (Biorevo, BZ-9000, Keyence) of Jurkat cells treated with Ir complexes **3a**, **5**, **6**, **7a**, **7b**, **7c**, and **7d** (50 μM) or peptides **9b**, **10b**, **11b**, **12b**, and **14b** at 37 °C for 1 h. (a) Bright image of control (in the absence of Ir complex), (b) emission image of control, (c) overlay image of control, (d) bright field image with **3a**, (e) emission image with **3a**, (f) overlay image of (d) and (e), (g) bright field image with **5**, (h) emission image with **5**, (i) overlay image of (g) and (h), (j) bright field image with **6**, (k) emission image with **6**, (l) overlay image of (j) and (k), (m) bright field image with **7a**, (n) emission image with **7a**, (o) overlay image of (m) and (n), (p) bright field image with **7b**, (q) emission image with **7b**, (r) overlay image of (p) and (q), (s) bright field image with **7c**, (t) emission image with **7c**, (u) overlay image of (s) and (t), (v) bright field image with **7d**, (w) emission image with **7c**, (x) overlay image of (v) and (w). (y) Overlay image of bright field and emission images with **3a** (25 μM) at 4 °C for 1 h. (z) Overlay image of bright field and emission images with **5** (10 μM) at 4 °C for 1 h. (aa) Overlay image of bright field and emission images with **6** (10 μM) at 4 °C for 1 h. (ab) Overlay image of bright field and emission images with **7a** (10 μM) at 4 °C for 1 h. (ac) Overlay image of bright field and emission images with **7b** (8 μM) at 4 °C for 1 h. (ad) Overlay image of bright field and emission images with **7c** (5 μM) at 4 °C for 1 h. (ae) Overlay image of bright field and emission image with **7d** (2 μM) at 4 °C for 1 h. (af)–(aj) Bright field images with **9b–12b**, and **14b** (1 mM) at 37 °C for 1 h. Excitation at 377 nm for Ir complexes. Scale bar (black) = 10 μm.

We next co-stained Jukat cells with IPHs (**3a** and **7d**) and fluorescence probes for intracellular organelle such as 7-aminoactinomycin D (7-AAD, a nucleus stain), LysoTracker Red (lysosome stain), MitoTracker Red (mitochondria stain), and ER-RFP (endoplasmic reticulum-red fluorescent protein) (ER stain) on confocal microscopy (Fig. 8). For co-staining with LysoTracker Red and MitoTracker Red, Jurkat cells were incubated with each probe at 37 °C for 30 min. After washing with PBS, the cells were again incubated in the presence of **3a**

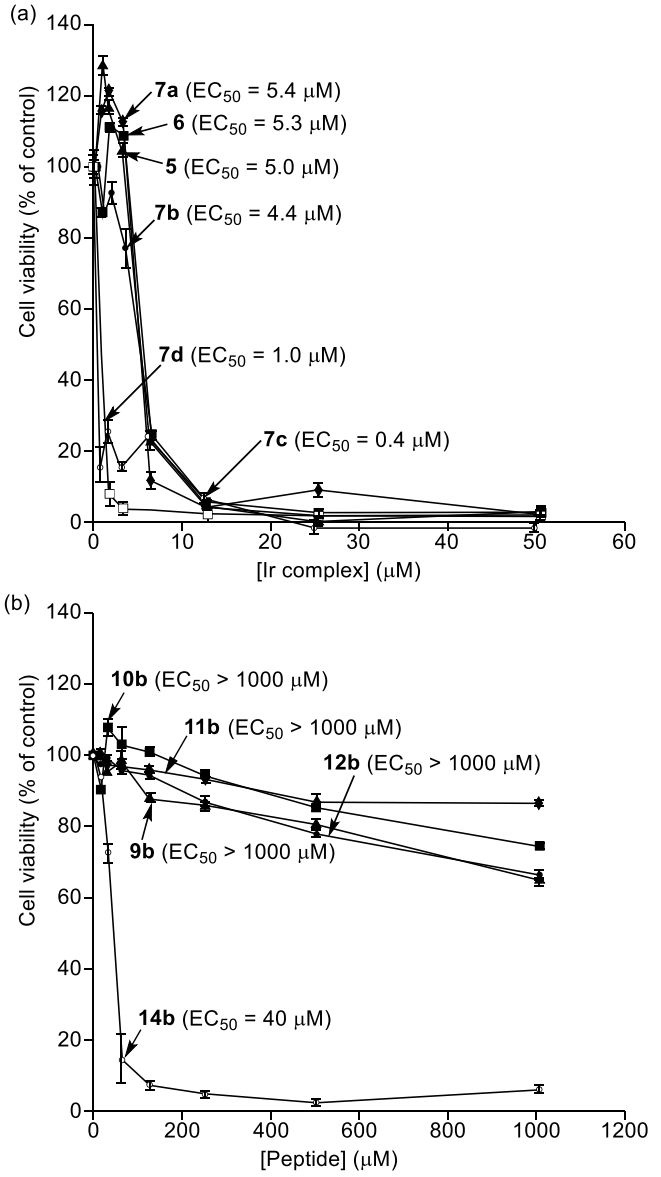

Fig. 3. (a) The results of MTT assays of Jurkat cells with **5** (filled triangles), **6** (filled squares), **7a** (filled diamonds), **7b** (filled circles), **7c** (open circles), and **7d** (open squares) in 10% FBS RPMI-1640 medium (incubation at 37 °C for 16 h). The net charge of these IPHs is assumed to be +9. (b) The results of MTT assays of Jurkat cells with peptides **9b** (filled triangles), **10b** (filled squares), **11b** (filled diamonds), **12b** (filled circles), and **14b** (open circles) in 10% FBS RPMI-1640 medium (incubation at 37 °C for 16 h). The net charge of these peptides is assumed to be +3.

Table 2
The EC_{50} values of Ir complexes **3a-c** and **5–7d** against Jurkat cells and IMR-90 cells. [a]Ref. 18.

Compound	EC_{50} against Jurkat cells	EC_{50} against IMR90 cells
3a	16 μM[a]	> 25 μM
3b	7.3 μM[a]	> 25 μM
3c	> 50 μM[a]	> 25 μM
5	(5.0 ± 1.1) μM	> 25 μM
6	(5.3 ± 0.4) μM	> 25 μM
7a	(5.4 ± 1.0) μM	> 25 μM
7b	(4.4 ± 0.5) μM	> 25 μM
7c	(0.40 ± 0.1) μM	(4.2 ± 1.1) μM
7d	(1.0 ± 0.4) μM	(7.2 ± 0.5) μM

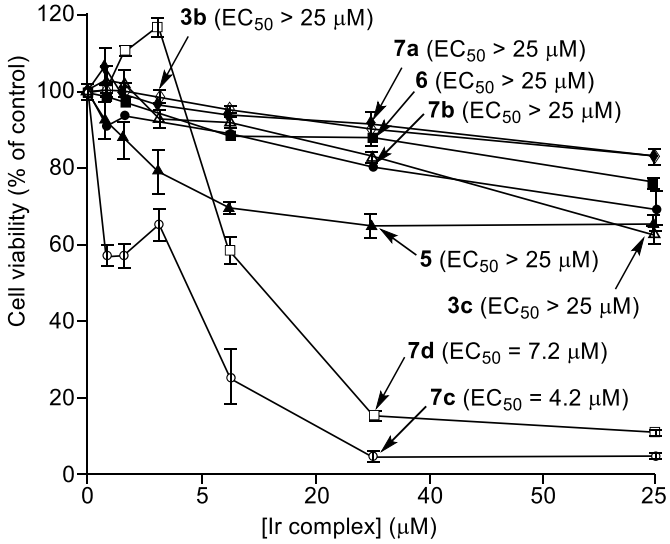

Fig. 4. The results of MTT assays of IMR-90 cells with **3b** (open diamonds), **3c** (open triangle), **5** (filled triangles), **6** (filled squares), **7a** (filled diamonds), **7b** (filled circles), **7c** (open circles), and **7d** (open squares) in 10% FBS RPMI-1640 medium (incubation at 37 °C for 24 h). The net charge of compounds is assumed to be +9.

(25 μM) or **7d** (10 μM) for an additional 1 h. For co-staining with ER-RFP, Jurkat cells were incubated with ER-RFP for 48 h and then incubated for 1 h in the presence of **3a** or **7d**. For co-staining with 7-AAD, 7-AAD and **3a** or **7d** were added to Jurkat cells at the same time, and the resulting mixtures were incubated at 37 °C for 1 h. Merged images for co-staining with 7-AAD (Fig. 8d,h) and MitoTracker Red (Fig. 8z,ad) show negligible overlap with the green emission of **3a** and **7d**, indicating that **3a** and **7d** are weakly localized in mitochondria. On the other hand, the emission of LysoTracker Red and ER-RFP was very weak in the presence of **3a** and **7d**, as shown in Fig. 8i–s and Fig. 8ae–ao, respectively. These findings suggest that the disappearance or structural breakdown of lysosomes and ER during the cell death process is activated by these IPHs.

As mentioned above, CaM was identified as one of the possible target proteins that are involved in cell death caused by **3a**, based on the proteomic analysis after photoaffinity labeling of Jurkat cells with **4** [19]. We were interested in determining whether **7d** induced the death of Jurkat cells through a Ca^{2+}-dependent pathway involving a Ca^{2+}-CaM complex. Time-lapse imaging of the intracellular Ca^{2+} response induced by **3b** and **7d** was conducted by fluorescent microscopy (**1a** (Scheme 1) was also used as a reference). Jurkat cells were initially stained with Rhod-4/AM, which is mainly localized in the cytoplasm, for 30 min, and microscopic fluorescence observations were initiated immediately after the addition of **1a** (50 μM), **3b** (50 μM) and **7d** (10 μM), respectively (**3b** was used in this experiment instead of **3a**, because the similar results of **3a** were already reported in our previous paper [18]). The fluorescent intensity of Rhod-4 was gradually enhanced in ca. 60% of the Jurkat cells during 10–40 min after the treatment with **3b**, as shown in Fig. 9c, while negligible change was detected in cells that were treated with non-toxic **1a** (Fig. 9a,b). The effect of **7d** (10 μM) on the cytosolic Ca^{2+} response was rapid and occurred immediately (within 0.5–2 min) after its addition (Fig. 9e). A careful observation of morphological and luminescent images revealed the immediate increase and then decrease in Ca^{2+} concentration after the addition of **7d** followed by membrane disruption, as shown in Fig. 9e and f.

The complexation of **7d** with CaM was next examined by 27 MHz QCM measurements. CaM was immobilized on a sensor chip and **7d** was then added. The complexation constants (K_{app}) (and disassociation constants (K_d)) for **7d** as well as **3a**, **8**, and **14b** with CaM, as determined from the ΔF decay curves, were $7.0 \times 10^5\ M^{-1}$ (K_d = 1.4 μM),

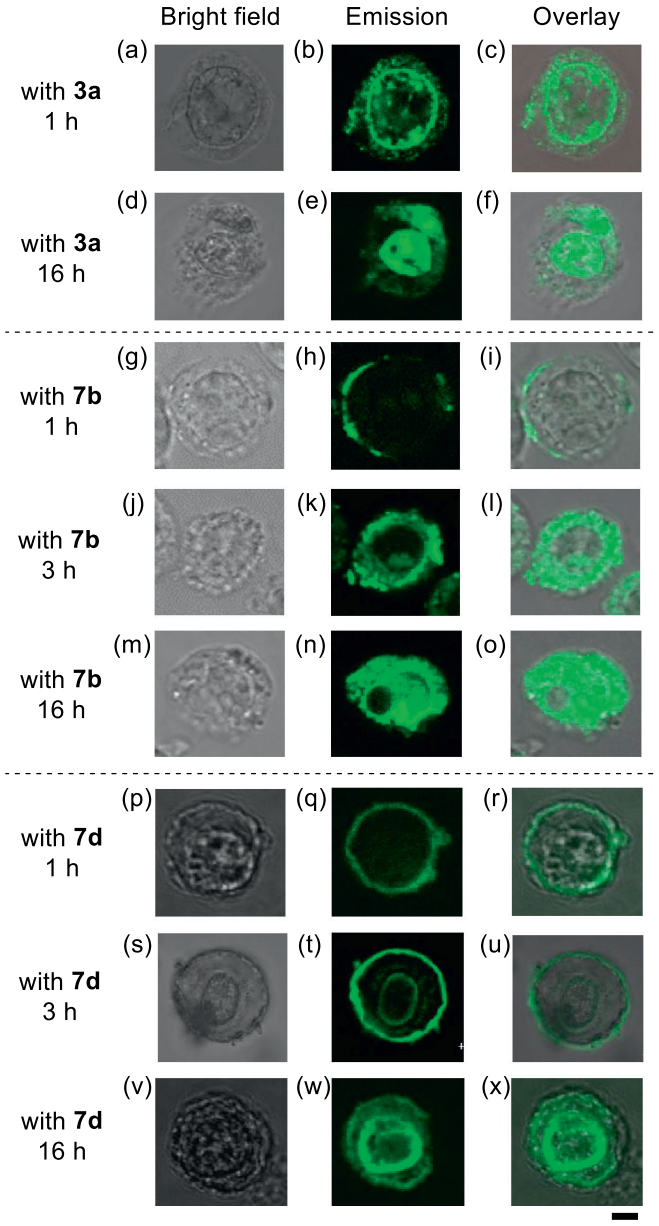

Fig. 5. Typical luminescent confocal microscopic images (Fluoview, FV-1000, Olympus) of Jurkat cells that had been treated with **3a** (25 μM), **7b** (10 μM), and **7d** (10 μM) for 1 h, 3 h, or 16 h at 37 °C. (a) Bright field image with **3a** for 1 h, (b) emission image with **3a** for 1 h, (c) overlay image of (a) and (b), (d) bright field image with **3a** for 16 h, (e) emission image with **3a** for 16 h, (f) overlay image of (d) and (e), (g) bright field image with **7b** for 1 h, (h) emission image with **7b** for 1 h, (i) overlay image of (g) and (h), (j) bright field image with **7b** for 3 h, (k) emission image with **7b** for 3 h, (l) overlay image of (j) and (k), (m) bright field image with **7b** for 16 h, (n) emission image with **7b** for 16 h, (o) overlay image of (m) and (n), (p) bright field image with **7d** for 1 h, (q) emission image with **7d** for 1 h, (r) overlay image of (p) and (q), (s) bright field image with **7d** for 3 h, (t) emission image with **7d** for 3 h, (u) overlay image of (s) and (t), (v) bright field image with **7d** for 16 h, (w) emission image with **7d** for 16 h, (x) overlay image of (v) and (w). Excitation at 405 nm for Ir complexes. Scale bar (black) = 2 μm.

$1.4 \times 10^5\,M^{-1}$ (K_d = 7.1 μM), $< 10^3\,M^{-1}$ (K_d > 1 mM), and $1.0 \times 10^5\,M^{-1}$ (K_d = 9.9 μM), respectively (Fig. 10 and Table 4). The K_d value of **7d** was greater than **3a**, although **7d** obviously has higher cytotoxic activity than **3a**, suggesting that relationship between the complexation of **7d** with CaM and cell death induction is weak. Note that the complexation of **7d** with CaM is attributed to its cationic peptide portion, because the Ir complex **8** without the cationic peptide part had a negligible affinity for CaM and the peptide alone **14b** binds weakly to CaM.

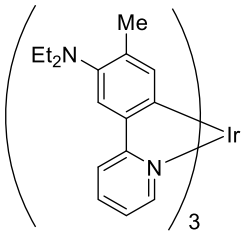

16

Scheme 5. Structure of Ir complex **16** which works as a pH sensor reported in our previous paper [25].

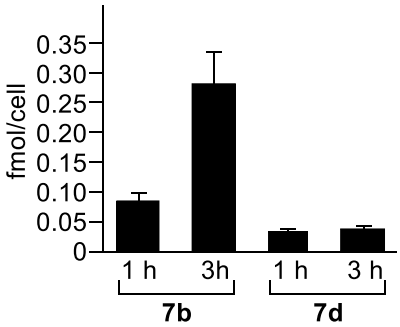

Fig. 6. Cellular uptake assay of iridium atom into Jurkat cells measured by ICP-MS after incubation with **7b** or **7d** (10 μM) at 37 °C for 1 or 3 h.

Table 3
The amount of iridium atom (fmol/cell) uptaken by Jurkat cells.

Compound	mol per cell (fmol/cell)
7b, 1 h	0.084 ± 0.01
7b, 3 h	0.28 ± 0.05
7d, 1 h	0.033 ± 0.002
7d, 3 h	0.040 ± 0.01

It is described that programed cell death can be classified into apoptosis, necroptosis, paraptosis, autophagic cell death, and so on [26–51]. In our previous study, we reported that cell death induced by **3a** (with a peptide at the 5′-position) was not inhibited by a broad caspase inhibitor, *Z*-VAD-fmk [18], while inhibition was observed in the presence some inhibitors related to Ca^{2+} homeostasis including 3-chlorophenylhydrazone (CCCP, an uncoupling reagent and an inhibitor of mitochondrial Ca^{2+} uptake) [44,45], verapamil (an L-type voltage-operated Ca^{2+} channel blocker) [46–48], quinidine (a Na^+ and K^+ channel blocker) [49,50] and xestospongin C (a selective inhibitor of the IP_3 receptor on the ER which releases Ca^{2+} into the cytosol) [51,52]. Based on these data, it was concluded that **3a** negligibly induces apoptosis but involves cell death that is mediated by Ca^{2+}-dependent signaling pathways.

To study the mechanism responsible for the cell death caused by **7d**, similar experiments were carried out. We observed the morphological changes in Jurkat cells that were treated with **3a** or **7d**, after the pre-treatment with benzyloxycarbonyl-VAD(OMe)-fluoromethylketone (Z-VAD-fmk), a pan-caspase inhibitor [42], or necrostatin-1, an inhibitor of the death domain receptor-associated adaptor kinase 1 (RIPK-1), namely a necroptosis inhibitor [43]. As shown in Figs. 11d-i and 10y-ad, both inhibitors showed negligible effects on the cytotoxicity of **3a** and **7d**, implying that apoptosis and necroptosis are not the major pathway of the cell death induced by **3a** and **7d**. The cells that were

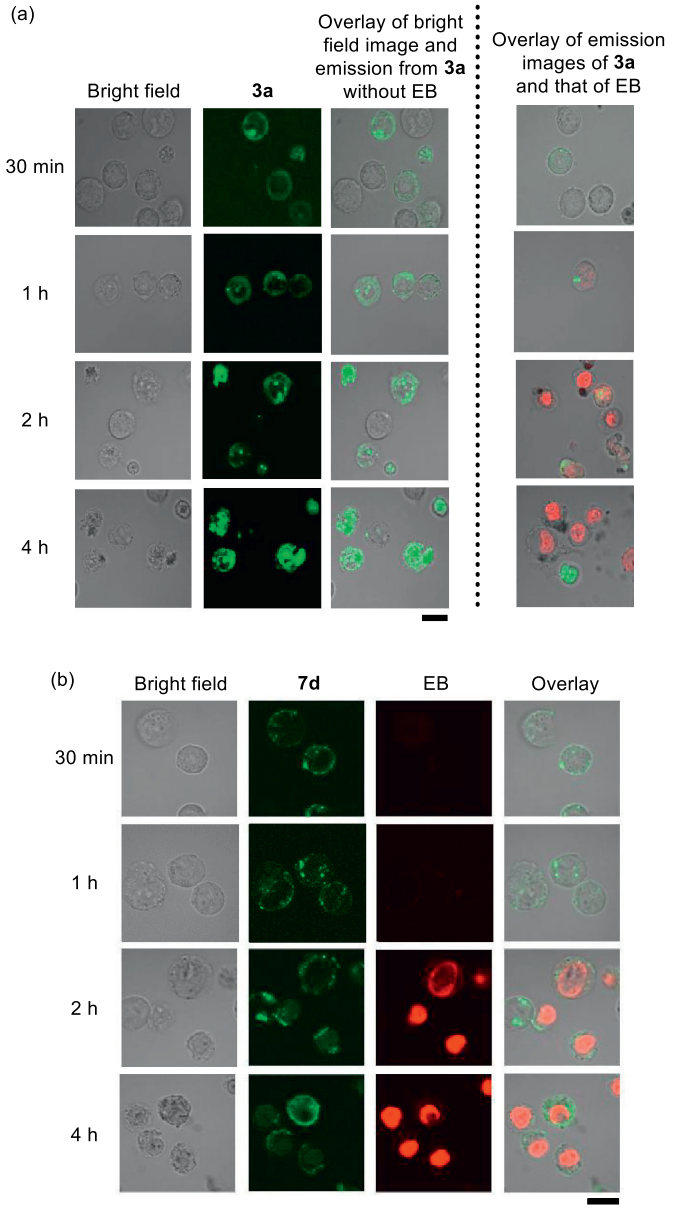

Fig. 7. Typical time-lapse images (Fluoview, FV-1000, Olympus) of Jurkat cells treated with (a) Ir complexes **3a** (10 μM) and (b) **7d** (1.6 μM) at 37 °C. Dead cells were stained (red emission) with ethidium bromide ([EB] = 127 μM). (a) Overlays of bright field and emission from **3a** in the absence or presence of EB are shown separately because green emission from **3a** was very weak in the presence of EB. Excitation at 405 nm for Ir complexes and 559 nm for EB. Scale bar (black) = 10 μm. (For interpretation of the references to colour in this figure legend, the reader is referred to the web version of this article.)

treated with **3a** in the presence of verapamil (20 μM), quinidine (100 μM), CCCP (40 μM), and xestospongin C (10 μM) showed only negligible morphological changes and very weak emission from the Ir complexes was detected, as reported by us (Fig. 11j–u). On the other hand, **7d** (10 μM) caused cell death and green emission was observed in the presence of these inhibitors (Fig. 11ae–ap), suggesting that the mechanism for the cell death caused by **7d** is somewhat different from that of **3a**.

In order to characterize the type of programmed cell death induced by **7d**, Western blot analyses of apoptosis and autophagy marker proteins were carried out. After incubating Jurkat cells with **7d** (1, 2.5, 5, 7.5, 10, and 20 μM) for 1 h at 37 °C, the cleavage of caspase-3 and poly (adenosine diphosphate-ribose) polymerase (PARP), which are proteins

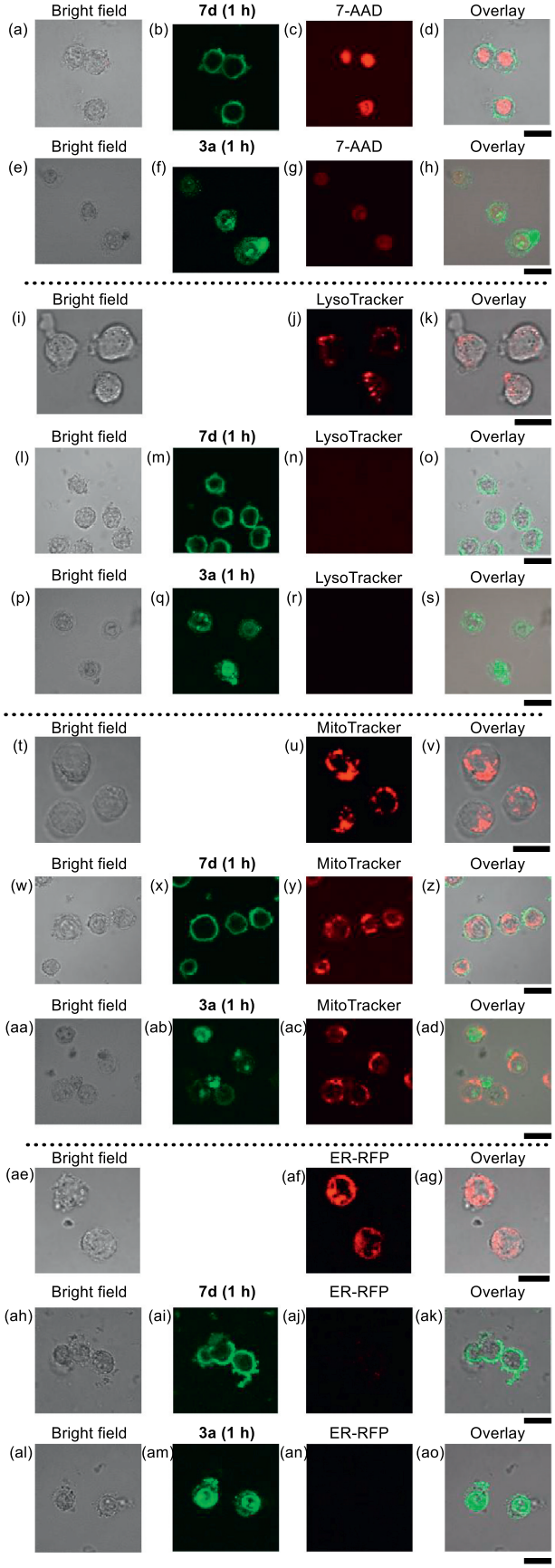

(caption on next page)

Fig. 8. Typical luminescent confocal microscopic images (Fluoview, FV-1000, Olympus) of Jurkat cells treated with 7-AAD, LysoTracker Red, MitoTracker Red and ER-RFP before or after incubation with **3a** (25 μM) and **7d** (10 μM) for 1 h. (a), (e), (i), (l), (p), (t), (w), (aa), (ae), (ah), and (al) Bright field images of Jurkat cells, (b), (m), (x) and (at) emission images with **7d**, (f), (q), (ab) and (am) emission images with **3a**, (c) and (g) emission images of 7-AAD, (j), (n), and (r) emission images with LysoTracker Red, (u), (y), and (ac) emission images with MitoTracker Red, (af), (aj), and (an) emission images with ER-RFP, (d) overlay image of (a–c), (h) overlay image of (e–g), (k) overlay image of (i–j), (o) overlay image of (l–n), (s) overlay image of (p–r), (v) overlay image of (t–u), (z) overlay image of (w–y), (ad) overlay image of (aa–ac), (ag) overlay image of (ae–af), (ak) overlay image of (ah–aj), and (ao) overlay image of (al–an). Excitation at 405 nm for (b), (f), (j), (n), (r), (v), (z), and (ad), 473 nm for (a), (e), (i), (m), (q), (u), (y), and (ac), and 559 nm for (c), (g), (k), (o), (s), (w), (aa), and (af). Scale bar (black) = 10 μm. (For interpretation of the references to colour in this figure legend, the reader is referred to the web version of this article.)

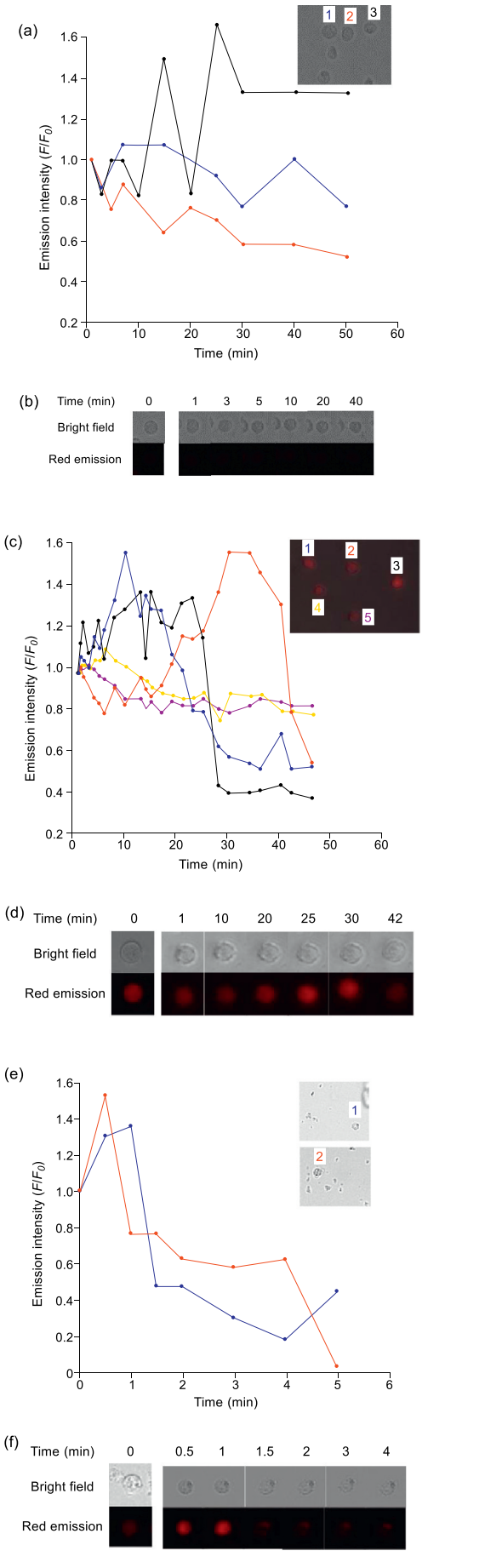

that are known to be activated during the apoptosis signaling pathway [53], were not observed under the same experimental conditions (Fig. 12a). In contrast, the upregulation of the microtubule-associated protein I light chain 3 (LC3)-I, II, the coiled-coil myosin-like Bcl-2-interacting protein-1 (Beclin-1), and an autophagy-related protein (Atg12), which are typical marker proteins for autophagy were observed [54–56], as displayed in Fig. 12b, supporting the conclusion that **7d** induces cell death via autophagy-type pathway and not apoptosis.

It is known that autophagy is required for homeostasis cellular maintenance and that it is upregulated in a various pharmacological stress conditions such as a lack of nutrients, viral/bacterial infections, hypoxia, DNA damage, low energy status, oxidative stress, ER and cellular stress [57–59]. It should be noted that autophagy is involved not only in self-protective mechanisms of cells, but also in programmed cell death [53].

Therefore, we examined the expression of proteins related to autophagy-inducing signals. It has been reported that autophagy is initiated by signaling pathways of growth factors such as the mammalian target of rapamycin (mTOR), ER stress, and other factors under intracellular stress conditions [58–63]. As shown in Fig. 12c, a Western blot analysis indicated that the levels of phosphorylation of extracellular signaling-regulated kinase 1/2 (ERK1/2) and c-Jun *N*-terminal kinase 1/2 (JNK1/2), proteins included mitogen-activated protein kinase (MAPK) family, were enhanced [64,65]. The expression of the CCAAT enhancer bunding protein (CHOP), which is generally known as an activator for apoptosis but also induces autophagy signaling in cases of ER stress [66–68], was activated by **7d**. On the other hand, **7d** showed only a negligible effect on the phosphorylation of mTOR. Based on these findings, the possibility arises that autophagic cell death is induced by **7d** via MAPK signaling pathways including ERK and JNK activation and not by the mTOR signaling pathway. It is known that the ERK signaling pathway is induced by Ras signaling pathway, ER stress and other processes modulate cell survival in response to extracellular stimuli [64,69]. Recent studies suggest that the roles of ERK activation in promoting cell death are complicated under certain conditions [70–73].

The effect of alkyl chain length at the *N*-terminus of the peptide portion in **7b–7d** on the cell membrane of Jurkat cells was examined by using giant liposomes consisting of lecithin (zwitterionic phospholipids such as a phosphatidylcholine prepared from egg yolk), as a model of a cell membrane (Fig. 13a). Phase contrast microscopic images indicate that **7d** (2 μM) induces considerable decomposition of liposome (Fig. 13d), while **7b** and **7c** induce negligible change (Fig. 13b,c). It was previously reported that **3b** and **3c** cause the decomposition of liposome, while **3a** exerts only a very weak effect [18]. The fact that the cytotoxicity of **3c** against Jurkat cells is weak suggests that the cytotoxic activity of **3a-c** is not proportional the length of the linker between the $Ir(tpy)_3$ core and the peptide parts. We conclude that longer

(caption on next page)

Fig. 9. (a) Time-lapse imaging of fluorescent changes of Rhod-4 loaded cells (F/F_0) after treatment with **1a** (50 μM). Curves depict the change in the emission of Rhod-4 from each cell (cell 1 (blue filled circles, blue plain line), cell 2 (red filled circles, red plain line), cell 3 (black filled circles, black plain line)). (b) Representative time-lapse images (Biorevo, Bz-9000, Keyence) of cell 2 in (a) (red filled circles, red plain line) after the treatment of **1a** (50 μM). (c) Time-lapse imaging of fluorescent changes in Rhod-4 loaded cells (F/F_0) after the treatment of **3b** (50 μM). Curves depict the change in the emission of Rhod-4 from each cell (cell 1 (blue filled circles, blue plain line), cell 2 (red filled circles, red plain line), cell 3 (black filled circles, black plain line), cell 4 (yellow filled circles, yellow plain line), cell 5 (purple filled circles, purple plain line)). (d) Representative time-lapse images of cell 2 in (c) (red filled circles, red plain line) after the treatment of **3b** (50 μM). (e) Time-lapse imaging of fluorescent changes in Rhod-4 loaded cells (F/F_0) after the treatment of **7d** (10 μM). Curves depict the change in the emission of Rhod-4 from each cell (cell 1 (blue filled circles, blue plain line), cell 2 (red filled circles, red plain line)). (f) Representative time-lapse images of cell 1 in (e) (blue filled circles, blue plain line) after treatment with **7d** (10 μM). Excitation at 540 nm for Rhod-4. F_0: initial emission intensity of Rhod-4, F: emission intensity of Rhod-4 after the treatment of Ir complexes. (For interpretation of the references to colour in this figure legend, the reader is referred to the web version of this article.)

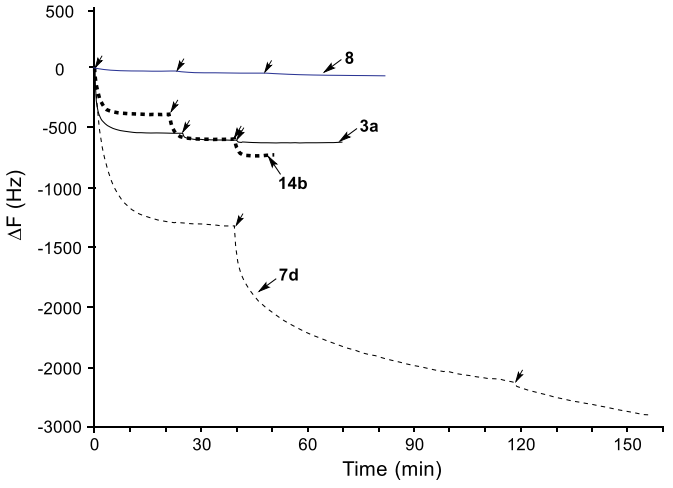

Fig. 10. Time course of frequency change (ΔF (Hz)) of binding between Ir complexes and CaM on 27 MHz QCM (Quartz Crystal Microbalance). Conditions: temperature: 25 °C, solvent: phosphate buffered saline (PBS). An aliquot of solutions of **3a** (6.6 μM/injection, black plain curve), **7d** (3.4 μM/injection, black plain dashed curve), **14b** (4 μM/injection, black bold dashed curve), **8** (1 μM/injection, blue plain curve) was added to CaM fixed on the sensor chip (single injection). Plain arrows indicate the time at which each compound was added to CaM. (For interpretation of the references to colour in this figure legend, the reader is referred to the web version of this article.)

Table 4
Complexation constants (K_{app}) and dissociation constants (K_d) for Ir complexes **3a**, **7c**, **8**, and peptide **14b** in PBS (pH = 7.4) at 25 °C.

Compound	K_{app} (M^{-1})	K_d (μM)
3a	1.4×10^5	7.1
7d	7.0×10^5	1.4
14b	1.0×10^5	9.9
8	$< 10^3$	> 1000

acyl groups at the *N*-terminus of the peptide portions exhibit strong interactions not only with the liposomal membrane but also with the cell membrane of Jurkat cells, as discussed above (Fig. 6 and Table 3). These results may indicate the possibility that **7d** induces necrosis-like cell death as well as autophagic cell death.

Based on the above results, a possible scheme for cell death signaling pathways induced by **7d** (and possibly **5**-**7a**,**b**,**c**) is presented in

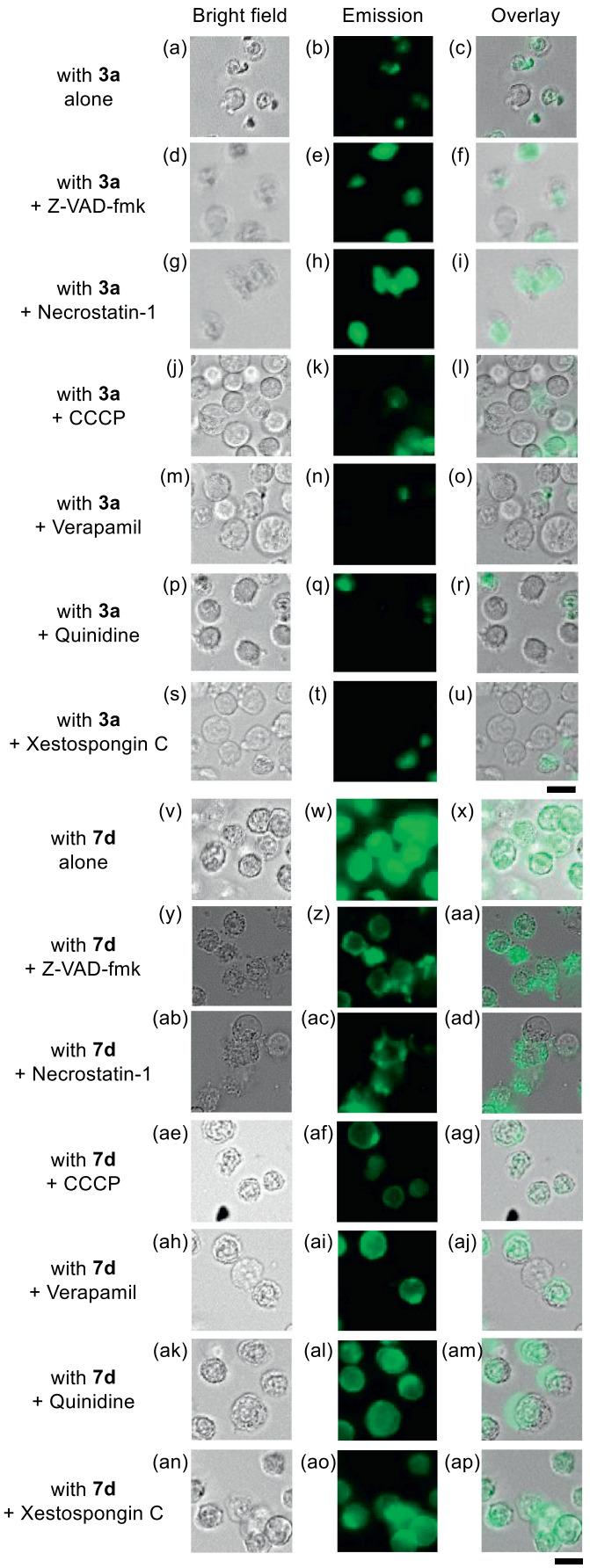

(caption on next page)

Fig. 11. Typical luminescence microscopic images (Biorevo, BZ-9000, Keyence) of Jurkat cells that were treated with **3a** (25 μM) and **7d** (10 μM) without any inhibitors (a–c for **3a**, v–x for **7d**) and in the presence of Z-VAD-fmk (15 μM) (d-f for **3a**, y-aa for **7d**), necrostatin-1 (30 μM) (g-i for **3a**, ab-ad for **7d**), CCCP (40 μM) (j–l for **3a**, ae–ag for **7d**), verapamil (20 μM) (m–o for **3a**, ah–aj for **7d**), quinidine (100 μM) (p–r for **3a**, ak–am for **7d**), and xestospongin C (20 μM) (s–u for **3a**, an–ap for **7d**) at 37 °C for 1 h. Excitation at 377 nm for **3a** and **7d**. Scale bar (black) = 10 μm.

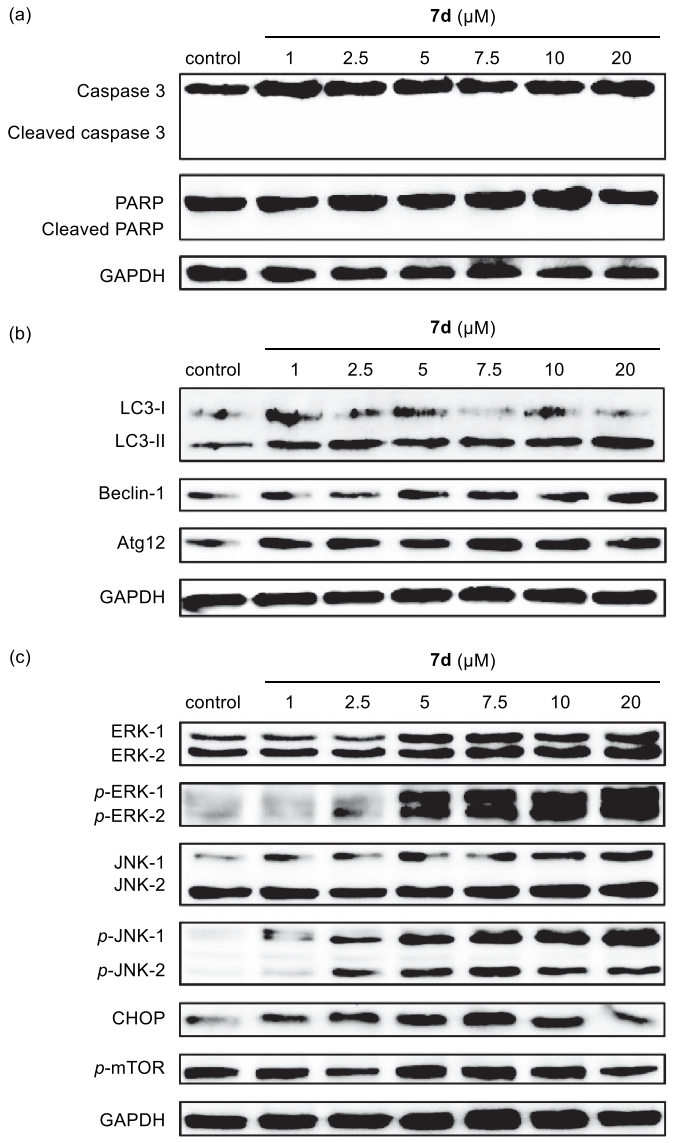

Fig. 12. Effect of **7d** on Western blot analysis. Jurkat cells were treated with different concentrations (1, 2.5, 5, 7.5, 10, and 20 μM) of **7d** for 1 h and the levels of expression of proteins were examined. (a) The expression of apoptosis related proteins, (b) the expression of autophagy related proteins, (c) the expression of ERK, JNK, and other related proteins. GAPDH is the endogenous control.

Scheme 6. There are two plausible upstream mechanisms for ERK and JNK activation, one of which is the Ras signaling pathway [74,75] and the second possibility is the ER stress signaling pathway [76–78]. It is known that the Ras signaling pathway, including ERK, is initiated by the activation of GPCRs, RTKs and extracellular stress [79,80]. Therefore, our hypothesis is that **7d** interacts with these cellular membrane receptors, thus damaging the ER. The lower cancer cell/normal cell selectivity for **7d** could be attributed to the breakdown of cell

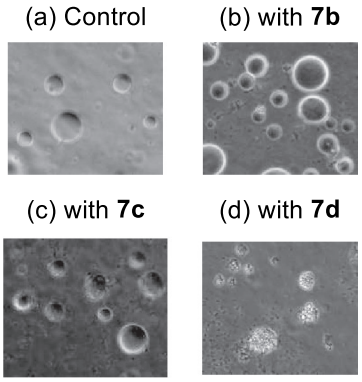

Fig. 13. Phase contrast images (Biorevo, Bz-9000 (Keyence)) of giant liposomes incubated in 10 mM HEPES buffer at pH 7.4 for 15 min (a) in the absence of Ir complexes or in the presence of (b) **7b** (2 μM), (c) **7c** (2 μM), or (d) **7d** (2 μM).

membranes (Fig. 13) by its hydrophobic alkyl chains at *N*-terminus of peptide portion (left side of Scheme 6).

3. Conclusion

In summary, we report herein that Ir complexes having hydrophobic acyl groups on the *N*-terminus of cationic KKKGG peptides induce cancer cell death more strongly than those of our previous IPHs such as **3a**, which contains no acyl group. Among the IPHs synthesized in this study, **7d** with *n*-heptadecanoyl groups exhibits considerable cytotoxicity against Jurkat cells. The microscopic imaging of Jurkat cells treated with **7d** and **3a** indicate that the cell death induced by these IPHs proceed via different signaling pathways. Namely, **3a** triggers the activation of the Ca^{2+}-dependent pathway and an intracellular Ca^{2+} response, possibly from mitochondria or the ER, via its movement to the cytosol and then to the interior of the nucleus. On the other hand, **7d** accumulates on the cell membrane and induces cell death via affecting the mitochondrial Ca^{2+}-independent pathways and then moves to the inside of the cytoplasm after incubation for long time (ca. 16 h). It should also be noted that **7a-d** which contain C3-C17 acyl groups at the *N*-terminus of the peptide portions also have potent anticancer activity against Jurkat cells, while our previous IPH **3c** with a C16 linker between the $Ir(tpy)_3$ core and the peptide units has a very weak cytotoxicity, possibly due to the structural difference between these IPHs.

Based on more detail mechanistic studies such as intracellular Ca^{2+} detection and Western blot analysis, in which the phosphorylation of ERK and JNK and upregulation of LC3-II, Beclin-1 and Atg12 were observed, we conclude that the cell death induced by **7d** includes autophagic cell death, necrosis-type cell death due to the interaction with cell membrane, and paraptosis via a Ca^{2+}-dependent signaling pathways based on our recent experimental results described elsewhere. The selectivity of the cytotoxicity of **7c** and **7d** for cancer versus normal is not high, possibly due to the interaction of their acyl parts at the *N*-terminus with the cell membrane. We thus conclude that the appropriate choice of alkyl structure at the *N*-terminus in the peptide units (such as **5**, **6**, **7a**, and **7b**) is important in terms of producing potent anticancer activity and good-high cancer/normal cells selectivity. This information would be useful for the design and synthesis of more useful IPHs and other peptides (and analogs) that function as potent anticancer agents and indicators of dead cells.

4. Experimental section

4.1. General information

All reagents and solvents were purchased at the highest commercial quality and were used without further purification. Anhydrous DMF

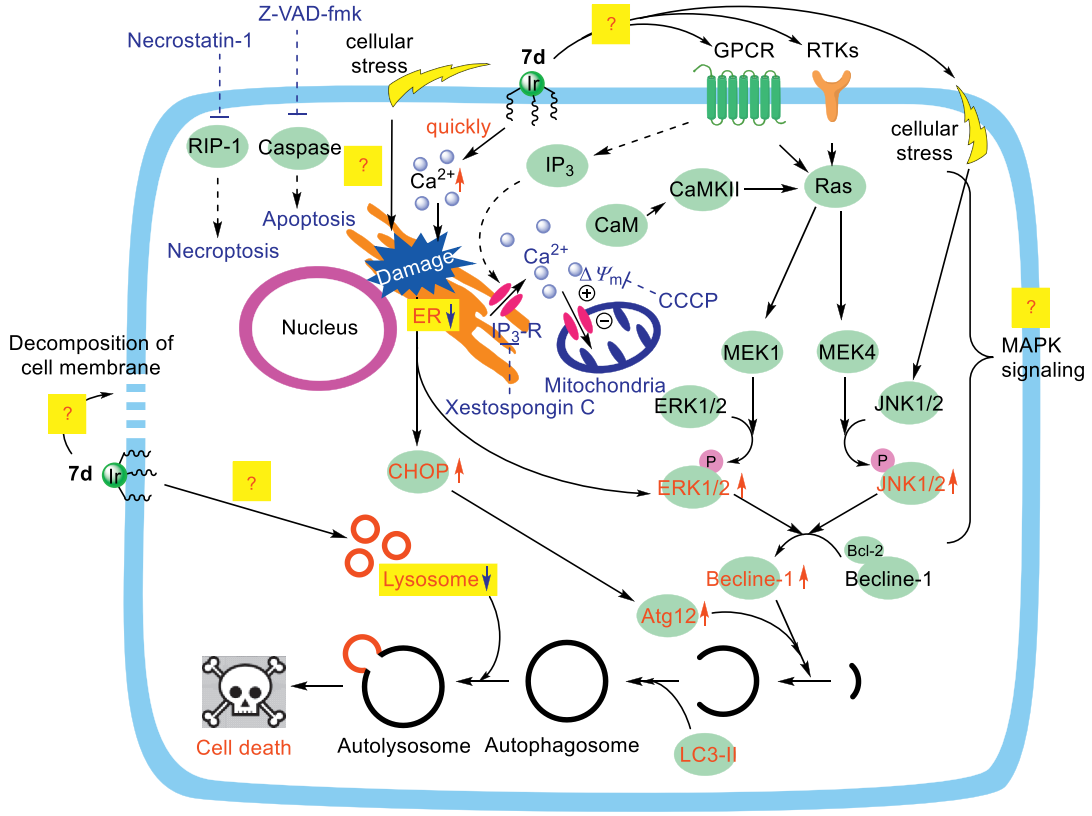

Scheme 6. Plausible mechanism for the cell death induced by **7d**. Red arrows indicate upregulation after the treatment with **7d**.

was obtained by distillation from calcium hydride. All aqueous solutions were prepared using deionized and distilled water. UV/vis spectra were recorded on a JASCO V-630 spectrophotometer at 25 °C. Emission spectra were recorded on a JASCO FP-6500 spectrofluorometer at 25 °C. IR spectra were measured on a Perkin-Elmer FT-IR spectrophotometer (Spectrum 100) at room temperature. ^{1}H (300 MHz and 400 MHz) NMR spectra were recorded on a JEOL Always 300 spectrometer and a JEOL Always 400 spectrometer, respectively. Luminescence imaging studies were performed using a fluorescent microscope (Biorevo, BZ-9000, Keyence) and a confocal microscope (Fluoview, FV-1000, Olympus). Tetramethylsilane (TMS) was used as an internal reference for ^{1}H NMR measurements in $CDCl_3$ and DMSO-d_6. 3-(Trimethylsilyl)-propionic-2,2,3,3-d_4 acid (TSP) was used as an internal reference for ^{1}H NMR measurements in D_2O. Mass spectral measurements were performed on a JEOL JMS-SX102A and Varian TQ-FT. The masses of some tris-cyclometalated Ir complexes were observed as $[M]^+$ (rather than $[M + H]^+$) in ESI electrospray ionization (ESI) mode (TQ-FT). Fast atom bombardment (FAB) mass spectra were recorded on a JEOL JMS-SX102A. Thin-layer chromatography (TLC) and silica gel column chromatography were performed using Merck Art. 5554 (silica gel) TLC plates and Fuji Silysia Chemical FL-100D, respectively. MTT was purchased from Dojindo. Z-VAD-fmk was purchased from Peptide Institute. Necrostatin-1 amd CaM (human recombinant, BML-SE325) was purchased from Enzo Life Science. Ethidium bromide, NaN_3, and $CaCl_2$ was purchased from Nacalai tesque. Verapamil hydrochlolide, xestospongin C, BSA, benzylpenicillin potassium, streptomycin sulfate, and monothioglycerol (MTG) were purchased from WAKO Pure Chemical Industries. Quinidine was purchased from TCI. CCCP was purchased from Sigma Aldrich. Quest™ Rhod-4/AM was purchased from AAT Bioquest. Caspase-3, PARP, ERK1/2, and *p*-ERK1/2 were purchased from Santa Cruz Biotechnology, USA. JNK1/2, p-JNK1/2, CHOP, LC3-I/II, Atg12, Beclin-1, mTOR, GAPDH, anti-rabbit and anti-mouse were purchased from Cell Signaling Technology, USA. HPLC analyses were carried out using a system consisting of a PU-2089 intelligent HPG pumps (JASCO, Japan), a UV-2075 Plus intelligent UV/vis detector (JASCO), a FP-2020 Plus intelligent fluorescence detector (JASCO), an injector (Model No. 7725i, Rheodyne), a USB chromatointerface unit (Model No. ADC44, LA soft, Japan), and a CDS software (ver. 5.0, LA soft). For analytical HPLC, a SenshuPak Pegasil ODS column (Senshu Scientific Co., Ltd.) (4.6ϕ × 250 mm, No. 6052602) was used. For preparative HPLC, a SenshuPak Pegasil ODS column (Senshu Scientific Co., Ltd.) (20ϕ × 250 mm, No. 0509271H) was used.

4.2. Synthesis

4.2.1. Synthesis of protected peptides

1-Adamantyl-HN-Lys(Boc)-Lys(Boc)-Lys(Boc)-Gly-Gly-CO_2H **9a**

Fmoc-Gly-2-Cl-Trt-Resin (0.20 g, 0.10 mmol) was deprotected by treatment with 20% piperidine/DMF. Each Fmoc-Xaa-OH (0.40 mmol) was then coupled at r.t. for 1 h to the Fmoc-deprotected resin in the presence of *N*,*N*'-diisopropylcarbodiimide (DIC) (62 μL, 0.40 mmol) and 1-hydroxybenzotriazole (HOBt) (0.11 g, 0.80 mmol) in dry DMF (1.0 mL). After repetition of the deprotection and coupling steps, 1-adamantylcarboxylic acid (54 mg, 0.30 mmol) was condensed with HBTU (0.15 g, 0.30 mmol) and DIEA (0.14 mL, 0.80 mmol). The protected peptide was cleaved from the resin using a solution of HFIP/CH_2Cl_2 (60/40) and stirred for 6 h. After separating the resin by filtration and washing several times with CH_2Cl_2 and MeOH, the resulting filtrate was concentrated under reduced pressure. The residue was re-precipitated by Et_2O and the insoluble compound was collected by filtration and washed with Et_2O to give **9a** as a colorless solid (44 mg, 45%). IR (ATR): 3279, 3087, 2975, 2930, 2854, 1687, 1626, 1517, 1453, 1392, 1365, 1248, 1166, 1037, 1009, 914, 863, 778, 646, 603, 562, 537, 509 cm^{-1}; ESI-MS (*m/z*) calcd for $C_{48}H_{82}N_8O_{13}$ $[M + Na]^+$: 1001.5897; found: 1001.5894.

Protected peptides **11a**, **12a**, and **13** were prepared according to the procedure used for **9a**

n-Propionyl-HN-Lys(Boc)-Lys(Boc)-Lys(Boc)-Gly-Gly-CO_2H **11a**:

Colorless solid (0.12 g, quant.). IR (ATR): 3283, 3076, 2977, 2931, 2862, 1682, 1631, 1525, 1452, 1404, 1391, 1365, 1276, 1249, 1167, 1102, 1037, 1012, 893, 864, 778, 684, 649, 610, 559, 537, 514 cm^{-1}; FAB-MS (*m/z*) calcd for $C_{40}H_{73}N_8O_{13}$ $[M + H]^+$: 873.5298; found: 873.5297.

n-Decanoyl-HN-Lys(Boc)-Lys(Boc)-Lys(Boc)-Gly-Gly-CO_2H **12a**:

Colorless solid (0.11 g, 89% yield). IR (ATR): 3282, 2928, 2859, 1684, 1631, 1525, 1455, 1441, 1414, 1393, 1366, 1278, 1250, 1167, 1103, 1039, 1014, 982, 893, 866, 842, 779, 685, 653, 616, 559, 515, 506, 493, 484, 465, 439, 431 cm^{-1}; FAB-MS (*m/z*) calcd for $C_{47}H_{86}N_8O_{13}Na$ $[M + Na]^+$: 993.6212; found: 993.6216.

n-Dodecanoyl-HN-Lys(Boc)-Lys(Boc)-Lys(Boc)-Gly-Gly-CO_2H **13**:

A colorless solid (0.13 g, quant.). IR (ATR): 3280, 3074, 2925, 2856, 1719, 1683, 1631, 1524, 1454, 1438, 1413, 1391, 1365, 1276, 1249, 1167, 1102, 1038, 1012, 980, 893, 865, 778, 701, 685, 648, 625, 597, 571, 561, 551, 540, 525, 511 cm^{-1}; FAB-MS (*m/z*) calcd for $C_{49}H_{90}N_8O_{13}$ $[M + Na]^+$: 1021.6525; found: 1021.6523.

n-Heptadecanoyl-HN-Lys(Boc)-Lys(Boc)-Lys(Boc)-Gly-Gly-CO_2H **14a**

The Fmoc-Gly-2-Cl-Trt-Resin (1.0 g, 0.65 mmol) was deprotected by treatment with a 20% piperidine/DMF solution. Each Fmoc-Xaa-OH (2.6 mmol) was coupled at r.t. for 1 h to the Fmoc-deprotected resin in the presence of DIC (0.40 mL, 2.6 mmol) and HOBt (0.70 g, 5.2 mmol) in dry DMF (5.0 mL). After repetition of the deprotection and coupling steps, H_2N-Lys(Boc)-Lys(Boc)-Lys(Boc)-Gly-Gly-CO_2H was stirred with *n*-heptadecanoic acid (0.26 mg, 1.9 mmol), 1-[bis(dimethylamino)methylene]-1*H*-benzotriazolium 3-oxide hexafluorophosphate (HBTU) (0.49 g, 1.9 mmol) and *N,N′*-diisopropylethylamine (DIEA) (0.90 mL, 5.2 mmol) in dry DMF/ CH_2Cl_2 (1/1) at room temperature for 2 h. The protected peptide was cleaved from the resin by treatment with a solution of 1,1,1,3,3,3-hexafluoro-2-propanol (HFIP)/CH_2Cl_2 (60/40) and stirred for 6 h. After separating the resin by filtration and washing several times with CH_2Cl_2 and MeOH, the resulting filtrate was concentrated under the reduce pressure. The residue was reprecipitated by Et_2O and the precipitation was filtrated to give **14a** as a colorless solid (0.56 g, quant.). IR (ATR): 3280, 3074, 2923, 2854, 1719, 1683, 1631, 1525, 1454, 1440, 1412, 1391, 1365, 1276,1249,1168, 1038, 1014, 980, 894, 865, 881, 778, 704, 684, 646, 616, 558, 543, 523 cm^{-1}; FAB-MS (*m/z*) calcd for $C_{54}H_{101}N_8O_{13}$ $[M + H]^+$: 1069.7489; found: 1069.7487.

4.2.2. Synthesis of deprotected peptides

1-Adamantyl-HN-Lys(NH_2)-Lys(NH_2)-Lys(NH_2)-Gly-Gly-CO_2H **9b**

1-Adamantyl-HN-Lys(Boc)-Lys(Boc)-Lys(Boc)-Gly-Gly-2-Cl-Trt-Resin was prepared in the same manner as described for **9a**. The protected peptide was cleaved from the resin and deprotected using TFA cocktail (TFA/H_2O/triisopropylsilane = 95/2.5/2.5) and stirred for 2 h. After separating the resin by filtration, the resulting filtrate was concentrated under the reduce pressure. The residue was reprecipitated by Et_2O and the precipitation was collected on a filter. The resulting filtrate was purified by preparative RP-HPLC (CH_3CN (0.1% TFA)/H_2O (0.1% TFA) = 0/100 to 50/50 (0 to 30 min), t_r = 15 min, 8.0 mL/min), lyophilized to give **9b** as a colorless amorphous (43 mg, 34% as 3TFA salt). IR (ATR): 3283, 3062, 2910, 2855, 2660, 1634, 1519, 1475, 1454, 1428, 1367, 1344, 1178, 1125, 1031, 978, 950, 912, 887, 836, 798, 721, 648, 597, 556, 516, 500 cm^{-1}; FAB-MS (*m/z*) calcd for $C_{33}H_{59}N_8O_7$ $[M + H]^+$: 679.4507; found:679.4507.

Deprotected peptides **10b**, **11b**, **12b**, and **14b** were prepared according to the procedure used for **9b**

Benzoyl-HN-Lys(NH_2)-Lys(NH_2)-Lys(NH_2)-Gly-Gly-CO_2H **10b**:

Colorless amorphous (88 mg, 74% as 3TFA salt). IR (ATR): 3278, 3062, 2939, 2873, 2549, 2342, 1973, 1731, 1634, 1577, 1526, 1491, 1428, 1336, 1170, 1131, 1029, 1002, 890, 837, 797, 721, 704, 653, 597, 516, 500 cm^{-1}; FAB-MS (*m/z*) calcd for $C_{29}H_{49}N_8O_7$ $[M + H]^+$: 621.3725; found: 621.3724.

n-Propionyl-HN-Lys(NH_2)-Lys(NH_2)-Lys(NH_2)-Gly-Gly-CO_2H **11b**:

Colorless amorphous (46 mg, 40% as 3TFA salt). IR (ATR): 3282, 3064, 2938, 2872, 1633, 1525, 1462, 1427, 1366, 1342, 1174, 1131, 1030, 951, 893, 837, 798, 721, 705, 654, 597, 557, 518, 489 cm^{-1}; FAB-MS (*m/z*) calcd for $C_{25}H_{49}N_8O_7$ $[M + H]^+$: 573.3725; found: 573.3724.

n-Decanoyl-HN-Lys(NH_2)-Lys(NH_2)-Lys(NH_2)-Gly-Gly-CO_2H **12b**:

Colorless amorphous (44 mg, 35% as 3TFA salt). IR (ATR): 3282, 3064, 2938, 2872, 1633, 1525, 1462, 1427, 1366, 1342, 1174, 1131, 1030, 951, 893, 837, 798, 721, 705, 654, 597, 557, 518, 481 cm^{-1}; FAB-MS (*m/z*) calcd for $C_{32}H_{63}N_8O_7$ $[M + H]^+$: 671.4820; found: 671.4820.

n-Heptadecanoyl-HN-Lys(NH_2)-Lys(NH_2)-Lys(NH_2)-Gly-Gly-CO_2H **14b**:

Colorless powder (29 mg, 20% as 3TFA salt). IR (ATR): 3288, 3072, 2920, 2851, 2553, 1933, 1779, 1665, 1627, 1535, 1467, 1430, 1402, 1355, 1178, 1131, 1030, 920, 837, 799, 721, 704, 598, 558, 551, 540, 517 cm^{-1}; FAB-MS (*m/z*) calcd for $C_{39}H_{77}N_8O_7$ $[M + H]^+$: 769.5916; found:769.5913.

4.2.3. Synthesis of IPHs

Ir complexes **3a** was synthesized according to our reported procedure [18].

Ir complex **5**

8 (20 mg, 13 μmol) was added to a solution of DIEA (49 μL, 0.25 mmol) in dist. DMF (44 μL). The reaction mixture was stirred at r.t. for 24 h. The reaction solution was precipitated by the addition of water and the insoluble product was collected by centrifugation. After purification by silica gel column chromatography ($CHCl_3$/MeOH = 10/1), the resulting product was collected as a yellow solid. A mixture of TMSCl (49 μL, 0.38 mmol) and NaI (57 mg, 0.38 mmol) in CH_3CN (0.25 mL) was added to the protected compound in CH_3CN (0.25 mL). The reaction mixture was sonicated for 5 min and then stirred at r.t. for 30 min. After deprotection, the insoluble compound was collected by centrifugation and washed with CH_3CN. The resulting residue was purified by preparative RP-HPLC (CH_3CN (0.1% TFA)/H_2O (0.1% TFA) = 20/80 to 60/40 (0 to 30 min), t_r = 14 min, 8.0 mL/min), lyophilized to give **5** as a yellow powder (8.1 mg, 15% as 9TFA salt from **8**). IR (ATR): 3281, 3061, 2929, 2856, 2553, 1774, 1633, 1524, 1473, 1426, 1303, 1262, 1133, 1070, 1022, 894, 836, 797, 783, 750, 721, 704, 684, 646, 616, 558, 543, 523 cm^{-1}; ^1H NMR (400 MHz, D_2O, TSP): δ = 8.03–7.95 (m, 3H), 7.85–7.75 (m, 6H), 7.65 (brs, 3H), 7.10–7.02 (m, 3H), 6.62 (s, 3H), 4.32–4.22 (m, 12H), 4.01–3.89 (m, 6H), 3.84 (s, 9H), 3.25–3.05 (m, 9H), 3.02–2.90 (m, 9H), 2.96 (brs, 21H), 2.10–2.03 (m, 9H), 1.95 (s, 9H), 1.92–1.52 (m, 93H), 1.50–1.20 (m, 60H) ppm.; ESI-MS (*m/z*) calcd for $C_{162}H_{256}N_{33}O_{21}{}^{191}Ir$ $[M + 4H]^{4+}$: 797.7394; found: 797.7390.

Ir complexes **6, 7a, 7b**, **7c**, and **7d** were prepared in a manner similar to that described for **5.**

Ir complex **6**: Yellow powder (5.1 mg, 11% as 9TFA salt from **8**). IR (ATR): 3278, 3061, 2931, 2860, 1662, 1635, 1579, 1531, 1472, 1427, 1302,11261, 1198, 1178, 1128, 1027, 950, 928, 891, 836, 799, 784, 750, 721, 704, 595, 559, 543, 517 cm^{-1}; ^1H NMR (300 MHz, D_2O, TSP): δ = 7.97 (brs, 3H), 7.75–7.73 (m, 9H), 7.62–7.44 (m, 15H), 7.03 (brs, 3H), 6.62 (s, 3H); 4.45–4.44 (m, 3H), 4.37–4.29 (m, 6H), 3.94 (d, *J* = 6.9 Hz, 6H), 3.82 (s, 6H), 3.30 (brs, 6H), 3.13–3.07 (m, 6H), 2.96–2.91 (m, 21H), 2.07 (s, 9H), 1.86–1.63 (m, 45H), 1.42–1.23 (m, 60H) ppm.; ESI-MS (*m/z*) calcd for $C_{150}H_{226}N_{33}O_{21}{}^{191}Ir$ $[M + 4H]^{4+}$: 754.1802; found: 754.1803.

Ir complex **7a**: Yellow powder (6.6 mg, 13% as 9TFA salt from **8**). IR (ATR): 3279, 3058, 2931, 2861, 1779, 1644, 1531, 1471, 1425, 1300, 1259, 1198,1173, 1128, 1069, 1022, 891, 834, 798, 720, 705, 591, 550, 515 cm^{-1}; ^1H NMR (400 MHz, D_2O, TSP): δ = 7.92 (d, *J* = 7.9 Hz, 3H), 7.69 (t, *J* = 7.9 Hz, 3H), 7.65 (s, 3H), 7.56 (d, *J* = 5.6 Hz, 3H), 6.96 (t, *J* = 6.0 Hz, 3H), 6.45 (d, *J* = 2.8 Hz, 3H); 4.20–3.97 (m, 3H), 3.81 (s, 9H), 3.70 (s, 9H), 3.25–3.20 (m, 9H), 3.05–2.90 (m, 12H), 2.83–2.75 (m, 33H), 2.18–2.15 (m, 9H), 1.99 (s, 9H), 1.75–1.52 (m,

79H), 1.38–1.19 (m, 87H), 0.96 (t, J = 7.5 Hz, 12H) ppm.; ESI-MS (m/z) calcd for $C_{138}H_{224}N_{33}O_{21}{}^{191}Ir$ $[M + 2H]^{2+}$: 1435.3543; found: 1435.3535.

Ir complex **7b**: Yellow powder (4.6 mg, 8.5% as 9TFA salt from **8**). IR (ATR): 3279, 3062, 2929, 2859, 1774, 1645, 1532, 1472, 1427, 1305, 1261, 1132, 1027, 892, 837, 798, 783, 750, 721, 705, 596, 517 cm^{-1}; ^1H NMR (400 MHz, DMSO-d_6, TMS): δ = 8.20 (t, J = 5.5 Hz, 3H), 8.13–8.05 (m, 9H), 8.01–7.93 (m, 12H), 7.85–7.80 (m, 9H), 7.74 (brs, 39H), 7.34 (d, J = 4.8 Hz, 3H); 7.14–7.11 (m, 3H), 6.59 (s, 3H), 4.22–4.17 (m, 15H), 3.91 (brs, 153H), 3.75–3.73 (m, 9H), 3.70–3.66 (m, 9H), 3.20–3.05 (m, 9H), 3.04–3.02 (m, 9H), 2.74 (brs, 24H), 2.15–2.11 (m, 6H), 2.08 (s, 9H), 1.51–1.47 (m, 54H), 1.37–1.23 (m, 108H), 0.85 (t, J = 6.7 Hz, 12H) ppm.; ESI-MS (m/z) calcd for $C_{159}H_{267}N_{33}O_{21}{}^{191}Ir$ $[M + 3H]^{3+}$: 1055.3481; found: 1055.3476.

Ir complex **7c**: Yellow solid (8.1 mg, 30% yield as 9TFA salt from **8**). IR (ATR): 3266, 3062, 2928, 2857, 1774, 1645, 1531, 1471, 1427, 1380, 1304, 1262, 1199, 1133, 1070, 1021, 893, 837, 798, 782, 750, 721, 704, 680, 673, 661, 645, 633, 592, 581, 572, 554, 545, 514 cm^{-1}; ^1H NMR (400 MHz, DMSO-d_6, TMS): δ = 8.21 (m, 6H), 8.13–8.08 (m, 12H), 8.02–7.96 (m, 12H), 7.84–7.82 (m, 9H), 7.79–7.66 (m, 45H), 7.42–7.34 (m, 6H), 7.15–7.10 (m, 3H), 6.59 (s, 3H), 4.25–4.23 (m, 15H), 3.05–3.00 (m, 6H), 2.78–2.62 (m, 21H), 2.75–2.37 (m, 6H), 2.08 (s, 9H), 1.75–1.56 (m, 12H), 1.56–1.38 (m, 63H), 1.56–1.38 (m, 63H), 1.23 (s, 165H), 0.87–0.83 (t, J = 7.0 Hz, 15H) ppm.; ESI-MS (m/z) calcd for $C_{165}H_{279}N_{33}O_{21}{}^{191}Ir$ $[M + 3H]^{+}$: 1083.3789; found: 1083.3809.

Ir complex **7d**: Yellow solid (26 mg, 28% yield as 9TFA salt from **8**). IR (ATR): 3282, 3061, 2925, 2855, 1774, 1645, 1531, 1471, 1426, 1378, 1301, 1259, 1199, 1174, 1130, 1070, 1023, 895, 835, 798, 782, 750, 720, 706, 596, 517 cm^{-1}; ^1H NMR (400 MHz, DMSO-d_6, TMS): δ = 8.21 (m, 3H), 8.13–8.08 (m, 9H), 8.02–7.95 (m, 12H), 7.83–7.70 (m, 45H), 7.36–7.35 (m, 3H), 7.15–7.11 (m, 3H); 6.59 (s, 3H), 4.22–4.15 (m, 12H), 3.74 (brs, 6H), 3.67 (d, J = 6.0 Hz, 6H), 3.20–3.14 (m, 12H), 3.05–3.00 (m, 12H), 2.75 (brs, 21H), 2.15–2.10 (m, 9H), 2.08 (s, 9H), 1.75–1.60 (m, 15H), 1.59–1.49 (m, 51H), 1.23 (s, 171H), 0.85 (t, J = 6.0 Hz, 12H) ppm.; ESI-MS (m/z) calcd for $C_{180}H_{310}N_{33}O_{21}{}^{191}Ir$ $[M + 4H]^{4+}$: 865.3444; found: 865.3447.

4.3. Measurements of photophysical properties (UV/vis absorption and luminescence spectra, emission lifetime and quantum yield)

UV/vis spectra were recorded on a JASCO V-630 spectrometer and emission spectra were recorded on a JASCO FP-6200 spectrofluorometer at 25 °C. Concentrations of all of the Ir complexes in stock solutions (PBS) were determined based on a molar extinction coefficient of 380 nm ($\varepsilon_{380\ nm}$ = (1.08 ± 0.07) × 10^4 M^{-1} cm^{-1}) of Ir complex **15** shown in Scheme 4 that was characterized by elemental analysis. Sample aqueous solutions in quartz cuvettes equipped with Teflon septum screw caps were degassed by bubbling Ar through the solution for 10 min prior to making the luminescence measurements.

The quantum yields for the luminescence (Φ) were determined by comparison with the integrated corrected emission spectrum of a quinine sulfate standard, whose emission quantum yield in 0.1 M H_2SO_4 was assumed to be 0.55 under the condition excited at 366 nm. Eq. (1) was used in calculating the emission quantum yields, in which Φ_s and Φ_r denote the quantum yields of the sample and reference compound, η_s and η_s are the refractive indexes of the solvents used for the measurements of the sample and reference, and A_s and A_r are the absorbance of the sample and reference, and I_s and I_r stand for the integrated areas under the emission spectra of the sample and reference, respectively.

$$\Phi_s = \Phi_r(\eta_s{}^2 A_r I_s)/(\eta_r{}^2 A_s I_r) \quad (1)$$

The luminescence lifetimes of sample solutions in degassed aqueous solutions at 298 K were measured on a TSP1000-M-PL (Unisoku, Osaka, Japan) instrument using THG (355 nm) of Nd: YAG laser, Minilite I (Continuum, CA, USA) as the excitation source. The signals were monitored with an R2949 photomultiplier. Data were analyzed using the nonlinear least-squares procedure.

4.4. Cell cultures

Jurkat cell line was cultured in RPMI-1640 medium supplemented with 10% heat-inactivated FBS, L-glutamine, HEPES, antibiotic mixture (penicillin/streptomycin, 69.9 mg/L and 139 mg/L, respectively) and MTG in humidified 5% CO_2 incubator at 37 °C.

4.5. Fluorescent microscopy studies of Jurkat cells with Ir complexes

Jurkat cells (1 × 10^5 cells/mL, 100 μL) were incubated in the presence of Ir complexes (2, 10, 25 or 50 μM) or peptides (1 mM) in RPMI-1640 medium with 10% FBS for 1 h under 5% CO_2 at 4 °C (on ice) or 37 °C. After incubation, the cells were washed twice with ice-cold PBS with 0.1% NaN_3 and 0.5% FBS, and observed by fluorescent microscopy (Biorevo, Bz-9000, Keyence) by using Greiner CELLview™ petri dish (35 × 10 mm). Emission images were observed by FF01 filter (excitation 377 nm, emission 520 nm).

4.6. MTT assay against Jurkat cells

Jurkat cells (1 × 10^5 cells/mL, 100 μL) were incubated in 10% FBS RPMI-1640 medium containing Ir complexes (0–50 μM) or peptides (0–1 mM) under 5% CO_2 at 37 °C for 16 h (or 1–4 h) on 96 well plates (BD Falcon), 0.5% MTT reagent in PBS (10 μM) was then added to the cells. After incubation at 37 °C for 4 h, a formazan lysis solution was added and the resulting solution was incubated overnight under the same conditions, followed by measurement of absorbance at 570 nm with a microplate reader (BIO-RAD).

4.7. MTT assay against IMR90 cells

IMR-90 cells (2 × 10^5 cells/mL, 100 μL) were incubated in 10% FBS RPMI-1640 medium containing solution of Ir complexes (0–25 μM) under 5% CO_2 at 37 °C for 24 h on 96 well plates (BD Falcon), 0.5% MTT reagent in PBS (10 μM) was then added to the cells. After incubation at 37 °C for 4 h, a formazan lysis solution was added and the resulting solution was incubated overnight under the same conditions, followed by measurement of absorbance at 570 nm with a microplate reader (BIO-RAD).

4.8. Fluorescent microscopy studies of Jurkat cells with Ir complexes in the presence of inhibitors

Jurkat cells (1 × 10^5 cells/mL, 100 μL) in RPMI-1640 medium with 10% FBS were pretreated with inhibitors under 5% CO_2 at 37 °C for 30 min and then Ir complexes (10 or 50 μM) were added into the cells. After incubation at 37 °C for 1 h, the cells were washed twice with ice-cold PBS with 0.1% NaN_3 and 0.5% FBS, and observed by fluorescent microscopy (Biorevo, Bz-9000, Keyence) by using Greiner CELLview™ petri dish (35 × 10 mm). Emission images were observed by FF01 filter (excitation 377 nm, emission 520 nm).

4.9. Fluorescent confocal microscopy studies of Jurkat cells with Ir complexes

Jurkat cells (1 × 10^5 cells/mL, 100 μL) were incubated in the presence of Ir complexes (10 or 25 μM) in RPMI-1640 medium with 10% FBS for 1 h under 5% CO_2 at 37 °C. After incubation, the cells were washed twice with ice-cold PBS with 0.1% NaN_3 and 0.5% FBS, and observed by confocal microscopy (Fluoview, FV-1000, Olympus) by using Greiner CELLview™ petri dish (35 × 10 mm). The excitation was at λ = 405 nm, and emission was at λ = 490–540 nm.

4.10. Measurement of cellular uptake of Ir complexes into Jurkat cells evaluated by ICP-MS

Jurkat cells (1.0×10^6 cells) were incubated with **7b** or **7d** (10 μM) under 5% CO_2 at 37 °C for 1 h ($n = 3$). The cells were collected by centrifugation (2000 rpm, 4 °C, 3 min) and washed with PBS three times, and then a 70% HNO_3 aq. (0.50 mL) was added and incubated at 4 °C for 24 h. After the centrifugation (15,000 rpm, 4 °C, 10 min), 0.40 mL of the supernatant was transferred to a 15 mL centrifuge tube with miliQ (9.6 mL) and then filtrated. These solutions are measured by ICP-MS to determine the concentration of iridium atom.

4.11. Time-lapse imaging of Jurkat cells treated with Ir complexes by fluorescent confocal microscopy

Jurkat cells (1×10^5 cells/mL, 100 μL) were incubated in the presence of Ir complexes (1.6 μM for **7c** or 10 μM for **3a**) in RPMI-1640 medium with 10% FBS for 30 min–4 h under 5% CO_2 at 37 °C. The treated cells were washed twice with ice-cold PBS with 0.1% NaN_3 and 0.5% FBS, and ethidium bromide in PBS was added for the detection of dead cells. 5 min after the addition of ethidium bromide, sample on Greiner CELLview™ petri dish (35 × 10 mm) was observed by confocal microscopy (Fluoview, FV-1000, Olympus). The excitation was at λ = 405 nm for Ir complexes, and λ = 559 nm for ethidium bromide. The emission was at λ = 490–540 nm for Ir complexes, and λ = 570–670 nm for ethidium bromide.

4.12. Fluorescent confocal microscopy studies of Jurkat cells treated with Ir complexes and 7-AAD

Jurkat cells (1×10^5 cells/mL, 100 μL) were incubated with Ir complexes in 10% FBS RPMI-1640 medium containing 7-AAD (1 μg/mL) (Invitrogen) for 1 h under 5% CO_2 at 37 °C. After the incubation, the cells were washed twice with ice-cold PBS with 0.1% NaN_3 and 0.5% FBS, and observed by confocal microscopy (Fluoview, FV-1000, Olympus) by using Greiner CELLview™ petri dish (35 × 10 mm). The excitation was at λ = 405 nm for Ir complexes, and λ = 559 nm for 7-AAD. The emission was at λ = 490–540 nm for the Ir complexes, and λ = 570–670 nm for 7-AAD.

4.13. Fluorescent confocal microscopy studies of Jurkat cells treated with Ir complexes and LysoTracker Red or MitoTracker Red

Jurkat cells (1×10^5 cells/mL, 100 μL) were incubated with LysoTracker Red (Invitrogen) or MitoTrecker Red (Invitrogen) in 10% FBS RPMI-1640 medium for 30 min under 5% CO_2 at 37 °C. Ir complexes were added, and the cells were incubated for a further 1 h. After the incubation, the cells were washed twice with ice-cold PBS with 0.1% NaN_3 and 0.5% FBS, and observed by confocal microscopy (Fluoview, FV-1000, Olympus) using a Greiner CELLview™ petri dish (35 × 10 mm). The excitation was at λ = 405 nm for Ir complexes, and λ = 559 nm for LysoTracker Red and MitoTracker Red. The emission was at λ = 490–540 nm for Ir complexes, and λ = 570–670 nm for LysoTracker Red and MitoTracker Red.

4.14. Fluorescent confocal microscopy studies of Jurkat cells treated with Ir complexes and ER-RFP

Jurkat cells (1×10^5 cells/mL, 100 μL) were incubated with CellLight™ ER-RFP, BacMam 2.0 (Invitrogen) (10 μL) in 10% FBS RPMI-1640 medium (500 μL) for 48 h under 5% CO_2 at 37 °C. Ir complexes were added, and the cells were incubated for a further 1 h. After the incubation, the cells were collected by centrifugation and observed by confocal microscopy (Fluoview, FV-1000, Olympus) by using Greiner CELLview™ petri dish (35 × 10 mm). The excitation was at λ = 405 nm for Ir complexes, and λ = 559 nm for ER-RFP. The emission was at λ = 490–540 nm for Ir complexes, and λ = 570–670 nm for ER-RFP.

4.15. Ca^{2+} measurement

To measure the cytoplasmic Ca^{2+} concentration, Jurkat cells (1×10^5 cells/mL, 100 μL) were incubated with Rhod-4/AM (5 μM) in Ca^{2+} free RPMI-1640-based buffer containing 103 mM NaCl, 5.4 mM KCl, 0.41 mM $MgSO_4$, 24 mM $NaHCO_3$, 5.6 mM Na_2HPO_4, 11 mM glucose, and 10 mM HEPES-NaOH (pH 7.4) for 30 min under 5% CO_2 at 37 °C, then washed twice with the same buffer, and replaced with RPMI-1640-based buffer containing 0.42 mM $CaCl_2$, 103 mM NaCl, 5.4 mM KCl, 0.41 mM $MgSO_4$, 24 mM $NaHCO_3$, 5.6 mM Na_2HPO_4, 11 mM glucose, and 10 mM HEPES-NaOH (pH 7.4). The loaded cell suspension was placed on a Greiner CELLview™ petri dish (35 × 10 mm) under 5% CO_2 at 37 °C and the change in the fluorescent intensity of Rhod-4 immediately after the addition of Ir complex was then observed by fluorescent microscopy (excitation 540 nm, emission 605 nm). Fluorescence intensity of the calcium probe was analyzed by means of a BZ analyzer II (Keyence).

4.16. Measurement of the complexation constants of Ir complexes and peptides with CaM by 27 MHz QCM experiment

QCM Analyses were performed on an Affinex-Q4 apparatus (Initium Inc., Japan). After cleaning the Au (4.9 mm^2) electrode, which was equipped with quartz crystal, with 1% SDS and piranha solution, it was incubated at room temperature for 60 min with an aqueous solution of 3,3′-dithiodipropionic acid (3 mM, 4 μL). The surface was washed with distilled water and then activated by treatment with a mixture of 1-ethyl-3-(3-dimethylaminopropyl)carbodiimide (EDC)-HCl (0.52 M) and *N*-hydroxysuccinimide (0.87 M) for 30 min, washed with distilled water, then treated with CaM (100 μg/mL, 5 μL) at room temperature for 1 h. After washing with distilled water, 1 M ethanolamine (5 μL) was added as a blocking reagent. After washing with distilled water, the cell was filled with PBS (500 μL). The apparent complexation constants (K_{app}) for the compounds with CaM in PBS were calculated from the decrease in frequency. The nonspecific response was subtracted from the frequency decrease curve to give the apparent complexation constants K_{app} and dissociation constants K_d ($= 1/K_{app}$).

4.17. Western blot analysis

Jurkat cells (3×10^6 cells/mL, 100 μL) were treated with the Ir complexes and incubated for 1 h at 37 °C and under atmosphere of 5% CO_2. After treatment, cells were washed twice with ice cold PBS and proteins were extracted by RIPA buffer (Nacalai Tesque, Japan). The extracted proteins were quantified by Pierce™ BCA Protein Assay Kit (Thermo Scientific). Proteins (50 μg/well) were used for SDS-PAGE (7.5–15%) (BioRad, USA). After the SDS-PAGE, the gel was transferred to a polyvinylidene fluoride membrane (Merck Millipore, Germany) using semi dry blotter (BioRad, USA). The membrane was blocked with Blocking One solution (Nacalai Tesque, Japan) for 30 min at room temperature. After blocking, the membrane was washed three times with TBS-T (5 min at each time) and incubated overnight with primary antibodies diluted in signal enhancer HIKARI- solution A (Nacalai Tesque, Japan), the membrane was washed three times with TBST the next day and incubated for 1 h at r.t. with secondary antibody such as anti-rabbit or anti-mouse diluted in signal enhancer HIKARI- solution B (Nacalai Tesque, Japan). The protein signal was spotted by Chemi-Lumi One Ultra solution (Nacalai Tesque, Japan) using ChemiDoc MP system (BioRad, USA).

4.18. Preparation of giant liposome

Giant liposomes were prepared from lecithin egg yolk (WAKO) according to a literature report [18,81]. The lipids (1.5 mg) dissolved in $CHCl_3$ (1 mL) were added to a 50 mL round-bottom flask. After adding MeOH (0.15 mL), 10 mM HEPES buffer (pH 7.4) (7 mL) was then carefully added along the flask walls. The organic solvent was removed by rotary evaporation by slow rotation under reduced pressure at 40 °C. An aqueous suspension (ca. 6 mL) of giant liposomes was obtained after evaporation. The resulting solution of giant liposomes (50 μL) was added to the 96 well plate and incubated with IPHs (2 μM) for 15 min, and then observed on fluorescent microscopy (Biorevo, BZ-9000, Keyence).

Acknowledgements

This work was supported by grants-in-aid from the Ministry of Education, Culture, Sports, Science and Technology (MEXT) of Japan (Nos. 22890200, 24890256, and 26860016 for Y.H., and Nos. 22390005, 24659011, 24640156, and 15K00408 for S.A.), the Uehara Memorial Foundation for Y.H. and "Academic Frontiers" project for private universities: a matching fund study from MEXT, and the TUS (Tokyo University of Science) fund for strategic research areas. We wish to thank Prof. Dr. Ryushin Mizuta and Prof. Takeshi Nakamura (Research Institute for Biomedical Sciences, Tokyo University of Science) for confocal microscopic observations and helpful discussions. We would also wish to express our sincere appreciation to Prof. Toshiyuki Kaji and Dr. Eiko Yoshida (Faculty of Pharmaceutical Sciences, Tokyo University of Science) for giving normal cell line IMR-90. We also wish to thank Ms. Fukiko Hasegawa, Ms. Noriko Sawabe, and Ms. Yuki Honda (Faculty of Pharmaceutical Sciences, Tokyo University of Science) for measurement of MS spectrometry, NMR, and elemental analysis, respectively.

References

[1] L. Flamigni, A. Barbieri, C. Sabatini, B. Ventura, F. Barigelletti, Top. Curr. Chem. 281 (2007) 143–203.
[2] S. Obara, M. Itabashi, F. Okuda, S. Tamaki, Y. Tanabe, Y. Ishii, K. Nozaki, M. Haga, Inorg. Chem. 45 (2006) 8907–8921.
[3] K. Mori, M. Tottori, K. Watanabe, M. Che, H. Yamashita, J. Phys. Chem. C 115 (2011) 21358–21362.
[4] G.L. Schulz, X. Chen, S.A. Chen, S. Holdcroft, Macromolecules 39 (2016) 9157–9165.
[5] Z. Yan, Y. Wang, J. Ding, Y. Wang, L. Wang, ACS Appl. Mater. Interfaces 10 (2018) 1888–1896.
[6] K. Xiong, Y. Chen, C. Ouyang, R.L. Guan, L.N. Ji, H. Chao, Biochimie. (2016) 186–194.
[7] A. Zamora, G. Vigueras, V. Rodrígues, M.D. Santana, J. Ruiz, Coord. Chem. Rev. 360 (2018) 34–76.
[8] E. Baggaley, J.A. Weinstein, J.A.G. Williams, Coord. Chem. Rev. 256 (2012) 1762–1785.
[9] I. Omae, Coord. Chem. Rev. 310 (2016) 154–169.
[10] H. Xu, R. Chen, Q. Sun, W. Lai, Q. Su, W. Huand, X. Liu, Chem. Soc. Rev. 43 (2014) 3259–3302.
[11] I. Omae, J. Organomet. Chem. 823 (2016) 50–75.
[12] K.K.-W. Lo, M.-W. Louie, K.Y. Zhang, Coord. Chem. Rev. 254 (2010) 2603–2622.
[13] K.K.-W. Lo, K.Y. Zhang, RSC Adv. 2 (2012) 12069–12083.
[14] S. Tobita, T. Yoshihara, Curr. Opin. Chem. Biol. 33 (2016) 39–45.
[15] T. Yoshihara, Y. Hirakawa, M. Hosaka, M. Nangaku, S. Tobita, J. Photochem. Photobiol. 30 (2017) 71–95.
[16] A.-A. Masum, Y. Hisamatsu, K. Yokoi, S. Aoki, Bioinorg. Chem. Appl. 7578965 (2018).
[17] A.-A. Masum, K. Yokoi, Y. Hisamatsu, K. Naito, B. Shashni, S. Aoki, Bioorg. Med. Chem. 26 (2018) 4804–4816.
[18] Y. Hisamatsu, A. Shibuya, N. Suzuki, T. Suzuki, R. Abe, S. Aoki, Bioconjug. Chem. 26 (2015) 857–879.
[19] Y. Hisamatsu, N. Suzuki, A.-A. Masum, A. Shibuya, R. Abe, A. Sato, S. Tanuma, S. Aoki, Bioconjug. Chem. 28 (2017) 507–523.
[20] K. Yokoi, Y. Hisamatsu, K. Naito, S. Aoki, Eur. J. Inorg. Chem. (2017) 5295–5309.
[21] S. Aoki, Y. Matsuo, S. Ogura, H. Ohwada, Y. Hisamatsu, S. Moromizato, M. Shiro, M. Kitamura, Inorg. Chem. 50 (2011) 806–818.
[22] R.S. Lott, V.S. Chauhan, C.H. Stammer, J. Chem. Soc. Chem. Commun. 11 (1979) 493–495.
[23] Our preliminary measurement of the molecular sizes of IPHs by dynamic light-scattering (DLS) instrument (Zeta Sizer Nano (ZSL), Malvern Instruments) suggested some aggregated forms of Ir complexes having a diameter of > 50 nm, which seems to be larger than the molecular size of their monomeric structures studied by molecular models. However, it seems that these aggregation has very weak or negligible effect on their photophysical properties such as emission quantum yields, which are almost same as those of **1a** and **3a**. It should be noted that the solubility of these IPHs in aqueous solutions is not problematic in this work.
[24] A.B. Tamayo, B.D. Alleyne, P.I. Djurovich, S. Lamansky, I. Tsyba, N.N. Ho, R. Bau, M.E. Thompson, J. Am. Chem. Soc. 125 (2003) 7377–7387.
[25] S. Moromizato, Y. Hisamatsu, T. Suzuki, Y. Matsuo, R. Abe, S. Aoki, Inorg. Chem. 51 (2012) 12697–12706.
[26] N. Festjens, T. Vanden Berghe, P. Vandenabeele, Biochim. Biophys. Acta 1757 (2006) 1371–1387.
[27] J. Hitomi, D.E. Christofferson, A. Ng, J. Yao, A. Degterev, R.J. Xavier, J. Yuan, Cell 135 (2008) 1311–1323.
[28] W. Zhou, J. Yuan, Semin. Cell Dev. Biol. 35 (2014) 14–23.
[29] M. Pasparakis, P. Vandenabeele, Nature 517 (2015) 311–320.
[30] P. Hirsova, G.J. Gores, Cell. Mol. Gastroenterol. Hepatol. 1 (2015) 17–27.
[31] W. Bursch, Cell Death Differ. 8 (2001) 569–581.
[32] D. Gozuacik, A. Kimchi, Oncogene 23 (2004) 2891–2906.
[33] S. Cagnol, J.-C. Chambard, FEBS J. 277 (2010) 2–21.
[34] Z. Yang, D.J. Klionsky, Nat. Cell Biol. 12 (2010) 814–822.
[35] B. Zhivotovsky, S. Orrenius, Cell Calcium 50 (2011) 211–221.
[36] F. Janku, J.J. Wheler, S.N. Westin, S.L. Moulder, A. Naing, A.M. Tsimberidou, S. Fu, G.S. Falchook, D.S. Hong, I.G. Laguna, R. Luthra, J.J. Lee, K.H. Lu, R. Kurzrock, J. Clin. Oncol. 30 (2012) 777–782.
[37] F. Sun, X. Xu, X. Wang, B. Zhang, Tumor Biol. 37 (2016) 15467–15476.
[38] D. Lee, I.Y. Kim, S. Saha, K.S. Choi, Pharmacol. Ther. 126 (2016) 120–133.
[39] X. Zhang, L. Yu, H. Xu, Autophagy 12 (2016) 1954–1955.
[40] A. Danese, S. Patergnani, M. Bonora, M.R. Wieckowski, M. Previati, C. Giorgi, P. Pinton, Biochim. Biophys. Acta 1858 (2017) 615–627.
[41] M.W. Harr, C.W. Distelhorst, Cold Spring Harb. Perspect. Biol. 2 (2010) a005579.
[42] E.A. Slee, H. Zhu, S.C. Chow, M. MacFarlane, D.W. Nicholson, G.M. Cohen, Biochem. J. 315 (1996) 21–24.
[43] A. Degterev, J. Hitomi, M. Germscheid, I.L. Ch'en, O. Korkina, X. Teng, D. Abbott, G.D. Cuny, C. Yuan, G. Wagner, S.M. Hedrick, S.A. Gerber, A. Lugovskoy, J. Yuan, Nat. Chem. Biol. 4 (2008) 313–321.
[44] D.F. Babcock, J. Herrington, P.C. Goodwin, Y.B. Park, B. hille, J. Cell Biol. 136 (1997) 833–844.
[45] P. Bernardi, Physiol. Rev. 79 (1999) 1127–1155.
[46] W.A. Catterall, J. Striessnig, Receptor sites for Ca^{2+} channel antagonists, Trends Pharmacol. Sci. 13 (1992) 256–262.
[47] G.H. Hockerman, B.Z. Peterson, B.D. Johnson, W.A. Cotterall, Annu. Rev. Pharmacol. Toxicol. 37 (1997) 361–396.
[48] D.J. Triggle, Biochem. Pharmacol. 74 (2007) 1–9.
[49] H.J. Motulsky, A.S. Maisel, M.D. Snavely, P.A. Insel, Circ. Res. 55 (1984) 376–381.
[50] K. Shibata, A. Hirasawa, R. Foglar, S. Ogawa, G. Tsujimoto, Circulation 97 (1998) 1227–1230.
[51] S. Miyamoto, M. Izumi, M. Hori, M. Kobayashi, H. Ozaki, H. Karaki, Br. J. Pharmacol. 130 (2000) 650–654.
[52] T. Oka, K. Sato, M. Hori, H. Ozaki, H. Karaki, Br. J. Pharmacol. 135 (2002) 1959–1966.
[53] S. Sperandio, I. de Belle, D.E. Bredesen, Proc. Natl. Acad. Sci. USA 97 (2000) 14376–14381.
[54] F.T. Andón, B. Fadeel, Acc. Chem. Res. 46 (2013) 733–742.
[55] E. Yamada, R. Singh, Diabetes 61 (2012) 272–280.
[56] L. Wu, Y. Zhang, C. Zhang, X. Cui, S. Zhai, Y. Liu, C. Li, H. Zhu, C. Qu, G. Jiang, B. Yan, ACS Nano 8 (2014) 2087–2099.
[57] B. Levine, G. Kroemer, Cell 132 (2008) 27–42.
[58] C. He, D.J. Klionsky, Annu. Rev. Genet. 43 (2009) 67–93.
[59] S. Srindharan, K. Jain, A. Basu, Cancers 3 (2011) 2630–2654.
[60] A.-C. Chao, Y.-L. Hsu, C.-K. Liu, P.-L. Kuo, J. Agric. Food Chem. 59 (2011) 2086–2096.
[61] R. Sano, J.C. Reed, Biochim. Biophys. Acta 1833 (2013) 3460–3470.
[62] D. Senft, Z.A. Ronai, Trends Biochem. Sci. 40 (2015) 141–148.
[63] Q. Shi, X. Song, Z. Liu, Y. Wang, Y. Wang, J. Fu, C. Su, X. Xia, E. Song, Y. Song, Chem. Res. Toxicol. 29 (2016) 1160–1171.
[64] M. Raman, W. Chen, M.H. Cobb, Oncogene 26 (2007) 3100–3112.
[65] M. Krishna, H. Narang, Cell. Mol. Life Sci. 65 (2008) 3525–3544.
[66] Y.-J. Shin, S.-H. Han, D.-S. Kim, G.-H. Lee, W.-H. Yoo, Y.-M. Kang, J.-Y. Choi, Y.C. Lee, S.J. Park, S.-K. Jeong, H.-T. Kim, S.-W. Chae, H.-J. Jeong, H.-R. Kim, H.-J. Chae, Arthritis. Res. Ther. 12 (2010).
[67] W. B'Chir, C. Chaveroux, V. Carraro, J. Averous, A.-C. Maurin, C. Jousse, Y. Muranishi, L. Parry, P. Fafournoux, A. Bruhat, Cell. Signal. 26 (2014) 1385–1391.
[68] L. Zhang, F. Ren, X. Zhang, X. Wang, H. Shi, L. Zhou, S. Zheng, Y. Chen, D. Chen, L. Li, C. Zhao, Z. Duan, Dis. Model. Mech. 9 (2016) 799–809.
[69] A.L. Patel, S.Y. Shvartsman, Development. 145 (2018).
[70] S. Sperandio, K. Poksay, I. de Belle, M.J. Lafuente, B. Liu, J. Nasir, D.E. Bredesen, Cell Death Differ. 11 (2004) 1066–1075.

[71] W.-B. Wang, L.-X. Feng, Q.-X. Yue, W.-Y. Wu, S.-H. Guan, B.-H. Jiang, M. Yang, X. Liu, D.-A. Guo, J. Cell. Physiol. 227 (2012) 2196–2206.
[72] M.J. Yoon, A.R. Lee, S.A. Jeong, Y.-S. Kim, J.Y. Kim, Y.-J. Kwon, K.S. Choi, Oncotarget 5 (2014) 6816–6831.
[73] L. He, K.-N. Wang, Y. Zheng, J.-J. Cao, M.-F. Zhang, C.-P. Tan, L.-N. Ji, Z.-W. Mao, Dalton Trans. 47 (2018) 6942–6953.
[74] Y.D. Shaul, R. Seger, Biochim. Biophys. Acta (2007) 1213–1226.
[75] S. Yang, G. Liu, Oncol. Lett. 13 (2017) 1041–1047.
[76] F. Urano, X.Z. Wang, A. Bertolotti, Y. Zhang, P. Chung, H.P. Harding, D. Ron, Science 287 (2000) 664–666.
[77] B.J. Tan, G.N.C. Chiu, Int. J. Oncol. 42 (2013) 1605–1612.
[78] N.J. Darling, S.J. Cook, Biochim. Biophys. Acta 1843 (2014) 2150–2163.
[79] M.A. Lemmon, J. Schlessinger, Cell 141 (2010) 1117–1134.
[80] J.A. Williams, B.J. Holtz, American Pancreatic association (2017) 1.
[81] A. Moscho, O. Orwar, D.T. Chiu, B.P. Modi, R.N. Zare, Proc. Natl. Sci. U.S.A. 93 (1996) 11443–11447.